

Mode of occurrence, Texture and Geochemistry of Magnetite in
Magnetite-Ilmenite and Magnetite-Apatite ore from Pathargora,
Singhbhum Shear Zone, Eastern India

Thesis submitted

for the partial fulfilment of Master of Science in Applied Geology

Rajdeep Mondal

Registration No.- 128264 of 14-15

Class Roll No. 001720402021

Examination Roll No- MGEO194021

Department of Geological Sciences

Jadavpur University

Under the supervision of

Dr. Dipak C. Pal

Professor

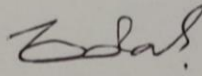
Department of Geological Sciences

Jadavpur University



FACULTY OF SCIENCE : DEPARTMENT OF GEOLOGICAL SCIENCES

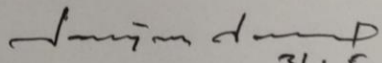
Certified that the dissertation entitled "*Mode of occurrence, texture and geochemistry of magnetite in magnetite-ilmenite and magnetite-apatite ore from Pathargora, Singhbhum Shear Zone, eastern India*" submitted by **Rajdeep Mondal** for the partial fulfilment of the M.Sc. Final Year, Final Semester Examination in Applied Geology, 2019, Jadavpur University embodies the results of studies carried out by him under my supervision and guidance. This work has not been submitted elsewhere for the award of any other degree.

 31.5.2019

Dr. Dipak C Pal
Professor
Department of Geological Sciences
Jadavpur University
Kolkata 700 032

Forwarded by

Dr. Dipak C. Pal
Professor
Dept. of Geological Sciences
Jadavpur University
Kolkata - 700 032, WB, INDIA

 31.5.18

Dr. Sanjoy Sanyal
Professor and Head
Department of Geological Sciences
Jadavpur University
Kolkata 700 032

Head
Department of Geological Sciences
Jadavpur University
Kolkata-700032

Dedicated to my ma and baba

Acknowledgement

At the forefront, I would like to thank my thesis supervisor and respected professor Dr. Dipak Chandra Pal for his continuous guidance, support and invaluable suggestions. I will never forget. Dr. Dipak Chandra Pal has been my inspiration as I hurdle all the obstacles in the completion of this research work.

I would like to thank Subhodip Adak for his constant and immense unselfish and unfailing support over these two years. He has always helped me to the greatest extent in academic purposes.

A special thanks to Abu Sayeed Baidya for enlighten me with his philosophical thoughts about various prospects.

The Department of Geological Sciences, Jadavpur University is thanked for providing all kind of support towards the completion of this work.

I must extend my sincere thanks to IIT-Kharagpur and everyone associated with SEM, EPMA and LA-ICP-MS analysis. The analytical expenditure is supported by Dr. Dipak C. Pal.

I must also thank my fellow classmate Ayan Sasmal, and seniors Sarthak Ghosh, Rupasree Saha and Souryadip Ghosh for helping me with every possibility. Without their participation and input, the validation work cannot be completed. I am surely going to miss all those the academic as well as non-academic discussions in the lab.

Finally, I must express my very profound gratitude to my parents and to my for providing me with unfailing support and continuous encouragement throughout my years of study. This accomplishment would not be possible without them.

Last but not least, I am ever thankful to my friend Surjyendu Bhattacharjee for helping me with literature survey.

Rajdeep Mondal
31.05.19

Abstract

The Singhbhum Shear Zone (SSZ) in the Eastern Indian Shield is known for its uranium and copper deposits. Multiple episodes of mineralization are reported from this Shear Zone (SSZ). Besides uranium and copper, several bodies of magnetite-apatite are reported from Singhbhum Shear Zone. However, there is no detailed work on textures and mode of occurrences of apatite-magnetite mineralization from this area. Magnetite, a common mineral in many different types of ore deposit ranging from skarn to BIF or porphyry to IOA (Iron-Oxide-Apatite) and IOCG (Iron-Oxide-Copper-Gold), is extensively used as a petrogenetic indicator due to its formation in a wide range of physico-chemical environment (including high-T magmatic conditions to low T hydrothermal conditions or metamorphic to sedimentary environment). Magnetite can incorporate different major or trace elements (Al, Ge, Ga, Mg, Ti, Zn, Co, V, Ni, Cr etc.) in its crystal structure depending on several intensive and extensive parameters like oxygen fugacity, temperature, partition co-efficient and compositions of the melt. In Pathargora, magnetite occurred mainly in two different modes. – 1. Magnetite (M1) associated with apatite-magnetite vein and 2. Massive magnetite body (M2). Both these types are hosted in feldspathic schist. Within massive magnetite body (M2), different kinds of ilmenite exsolution lamellae are observed. Major and trace element geochemistry clearly points to different formation conditions and processes are involved behind the origin of the two types of ore described here. Bivariate plots of V vs Ti (Cr (ppm) vs Ti (ppm), Ga (ppm) vs V (ppm) etc. shows distinct chemical differences between massive magnetite body (M2) relative to magnetite of apatite-magnetite vein (M1). Some widely used discrimination plots like Ti (ppm) vs Ni/Cr and Ni/(Cr+Mn) vs (Ti+V) wt% indicate different genesis mechanisms for these two different types of magnetite ore. Depending on trace element concentrations, element redistributions between magnetite and ilmenite during sub-solidus oxidation are noted.

Content

<u>Chapter</u>	<u>Page No.</u>
Chapter 1: Introduction	1-2
Origin of the problem	1
Objective vis-à-vis methodologies of the Study	2
Scope of the present study	2
Chapter 2: Regional Geology	3-10
Singhbhum Craton	3-4
North Singhbhum Mobile Belt (NSMB)	4-5
Chotanagpur Gneissic Complex (CGC)	5-6
Singhbhum Shear Zone (SSZ)	6
Local Geology	7-8
Chapter 3: Description of host rock, mode of occurrence and texture of ore minerals	11-22
Introduction	11
Magnetite-Apatite bearing feldspathic schist	11-13
Magnetite-ilmenite \pm apatite-bearing host feldspathic schist	13-15
Chapter 4: Geochemistry of Magnetite	23-27
Introduction	23
Methodology and Analytical Procedure	23
Mineralogy of Magnetite and Ilmenite	24
Major Element Geochemistry of Magnetite	24-26
Chapter 5: Trace Element Geochemistry of Magnetite	28-34
Introduction	28
Analytical Procedure	28
Trace element Geochemistry	29
Discriminant Diagram	29-30
Multielement Variation Diagram	30

Chapter 6: Discussion and Summary	35-38
Introduction	35
Ilmenite lamella: primary vs. secondary exsolution	35-36
Explanations for compositional variations among different types of magnetite	36-37

References

Chapter 1: Introduction:

1.1 Origin of the problem:

The ~200 km long arcuate intensely deformed Singhbhum Shear Zone (SSZ) in East Indian shield is important for its several polymetallic deposit, mined mainly for copper, uranium along with magnetite, gold, silver, copper, nickel as by-product. The SSZ separates Archean cratonic nucleus to the south from a Mesoproterozoic North Singhbhum Fold belt in the north. The iron oxide sulfide rich mineral deposits are mainly hosted in the hydrothermally altered, metamorphosed deformed rocks. The proposed ore genetic model of polymetallic mineralization in the SSZ vary widely from magmatic (Dunn and Dey, 1942), metamorphogenic related to migmatization (Talapatra, 1968) to volcanogenic massive sulfide deposits (VMS; Sarkar and Deb, 1974; Sarkar 1984) and IOCG type deposits (Pal et al., 2009). Previous studies propose multiple stages of mineralization prior to the shear zone formation (Sarkar, 1984; Pal et al. 2009, 2010, 2011).

Apatite-magnetite mineralization was the only source of phosphatic ore in the eastern India (Sarkar, 1984). These apatite-magnetite orebodies are almost concordant with regional schistosity. In addition, there are massive magnetite orebodies which are practically devoid of apatite. Detailed study on the mode of occurrence, texture and geochemistry of this massive magnetite vis-à-vis apatite-magnetite bodies is unavailable which hinders proper understanding of the origin and evolution of these ores.

Recent studies shows that magnetite can be used as petrogenetic indicator (Dupuis and Beaudoin, 2011; Dare et al. 2014) as they form under a wide array of physico-chemical condition. This study focuses on documentation of different mode of occurrences, texture and compositional variation of these magnetite from Pathargora, Singhbhum Shear Zone, Eastern India. Based on these parameters, this study attempts to address the probable origin of these magnetite in the massive magnetite and apatite-magnetite ores.

1.2 Objective vis-à-vis methodologies of the Study:

In accordance with the lacunae in our understanding of the nature and origin of the magnetite in different association the objective of the present work is as follows:

1. Understanding the mode of occurrences and distribution of the magnetite ore in the study area based on field and hand specimen study of the ores and their host rocks.
2. Identification of ore and associated minerals and deciphering their textural relations integration optical microscopy and scanning electron microscopy
3. Major and trace element characterization of magnetite and ilmenite using electron probe micro analyzer (EPMA) and Laser-ablation-inductively coupled plasma mass spectrometry (LA-ICP-MS) for a better insight into the origin of magnetite in different association.

1.3 Scope of the present study:

This study focuses on the textural association, major and trace element composition of magnetite and ilmenite from different mode of occurrences. This study therefore, provides the nature of different association of magnetite and ilmenite. Composition of any mineral is the indicator of the chemical ambience in which it form. Hence, composition of magnetite provide the information about the chemical ambience. Later alteration and oxidization of magnetite may obscures the primary features to some extent. Therefore, the primary composition of the magma and hydrothermal fluid from which different magnetite crystallize cannot be precisely well understood and beyond the scope of the study. An attempt is made to understand trace element redistribution/partitioning between magnetite and ilmenite to gain an idea about primary composition of melt.

2.1 Regional geology:

Singhbhum craton covers a triangular area of 50,000 sq.km and consists of a core of Singhbhum granite, rimmed by supracrustals of varied character and age.

The lithological associations are briefly outlined below:

2.2 Singhbhum Craton:

The oval-shaped singhbhum granite is a composite of several bodies which are assigned to three phases (phases I,II, and III). The phases I and II are geochemically distinguished as Type-A of Singhbhum granite called SBG-A (~300-3400 Ma), and phase III as Type-B (SBG-B, ~3100 Ma). Broadly, Singhbhum granite belongs to granodiorite-adamellite-granite suite, containing ~3500-~3600 Ma old enclaves of older metamorphic gneiss (OMG) and older metamorphic tonalitic gneiss (OMTG). The OMG comprises amphibolite facies pelitic schists, arenites, calc-magnesian meta sediments, ortho- and para- amphibolites etc. Of these, the pelitic schists are the most dominant suite with the other important rock types being muscovite-biotite (-sillimanite) schist, quartz sericite schist grading into quartzite and quartz-magnetite-cummingtonite schist. The OMTG rocks comprises a suite of biotite-hornblende tonalite gneiss, that grades into trondhjemite or granodiorite at places. The OMG rocks display evidence of intense deformation and metamorphism. The estimated P-T condition of peak metamorphism is 5-5.5 kb and 600-630°C temperature, indicating a substantial crustal thickening event (Saha, 1994).

The phase-I plutonic unit are K₂O poor granodiorite to tonalite, phase-II units are largely granodioritic while phase-III rocks are generally granitic with the highest average K₂O and SiO₂. Further based on the REE content, phases-I and -II are considered as SBG-A with slightly depleted HREE and no Eu anomaly while phase -III with LREE enriched nature and strong negative Eu anomaly is considered as SBG-B (Saha and Ray, 1984; Saha 1994).

The iron ore provinces of the Singhbhum craton consist of BIFs associated with metasedimentary and metavolcanic rocks which is together referred to as the Iron Ore Group (IOG). The major iron ore bearing provinces are the Badampahar-Gorumahisani belt in the east and north-east (IOG-I), Jamda-Koira-Noamundi belt of the west (IOG-II) and the Tomka-Daitaribelt in the south (IOG-III). IOG-I and-III have BIF associated with thick sequence of quartz arenite, fuchsite quartzite,

basic flows, tuff, chert and conglomerate while IOG-II comprises BIF that is overlain by shale and subordinate volcanics and underlain by shale and basic volcanics, local dolostone, sandstone and conglomerate. The IOG rocks have suffered lower greenschist facies metamorphism. Although a point of some controversy, most workers consider all the units of the iron ore provinces as part of the IOG and to be contemporaneous as well as older than the SBG-B (3.1 Ga) based on the ample evidence of profuse intrusion relation of SBG into the BIF sequences (Sarkar and Gupta, 2012).

Volcanic basins of variable ages occur in the craton and marginal orogen. Simlipal and Dhanjori volcanics are located in the eastern part of the shield, where Dhanjori is flanked by marginal Singhbhum Shear Zone orogen. Jagannathapur and Malangtoli basins are overlying Singhbhum granite in the west.

A prominent basic dyke swarm were named Newer Dolerite by Dunn and Dey (1942) trending in a dominant NNE to NE and a subordinate NW direction. These dykes traverse the entire craton. The dyke range in width from 10 cm to 1km and length varies over a few meter to 20km, and have on the average spacing of one to four km. The dykes are predominantly dolerites. Other types of dykes are peridotites , norites and lamprophyres.

2.2. North Singhbhum Mobile Belt (NSMB)

The NSMB is considered to extend over the area between the Singhbhum craton in the south and the Chotanagpur Gneissic Complex (CGC) in the north. In its southern most part it consists of the early Proterozoic sediment cover now metamorphosed in greenschist to amphibolite facies.

This meta-sedimentary belt contains polymictic conglomerate close to its basement and is overlain by low-grade meta-pelites, banded magnetite-quartz, tuffaceous rocks and mafic-ultramafic intrusives. In its eastern and western extremities the belt contains intra-cratonic sub-basins of the volcano-sedimentary suites of the Dhanjori and Ongarbira respectively. The Dhanjori sequence consists of phyllite, gritty shale, rhyolite porphyry, quartz-pebble conglomerate (QPC) interlayered with mafic-ultramafic units and finally overlain by quartzite and polymictic quartzite. The Ongarbira volcanic suite comprises K-poor tholeiite, high-Mg basalt, gabbro-pyroxenite

intrusives, basic tuffs and acid volcanics which are underlain by the meta sediments consisting of slate-phyllite, psammopelite, quartzite and dolomitic limestone.

To the north of this metasedimentary belt is the Singhbhum Shear Zone. Further north of the SSZ and south of the Dalma volcanics is another metasedimentary belt comprising a thick sequence of metapelites with minor meta-psammitic interbeds and profuse amphibolite, hornblende schist and quartzite bands. This belt is known as the Chaibasa Formation. Along the northern edge of this belt occurs the Dhalbhum formation and is composed of magnetitic phyllite with prominent quartzite bands. The major rock type of the Chaibasa is garnetiferous muscovite quartz schist with an estimated peak metamorphic condition of 3-6 kb and 415-600° C. A characteristic sub-ordinate rock type is kyanite-quartz rocks. The major rock type of the Dhalbhum are phyllites containing large porphyroblasts of andalusite and staurolite. To the north of Dhalbhum formation lies the arcuate ridge formed by the volcano-sedimentary rocks of the Dalma belt. The belt is composed of greenstone grade rocks of slate-phyllite, and carbonaceous phyllite/tuff interbedded with basic volcanics and overlain by thick sequence of Mg-rich volcanoclastics and co-magmatic komatiitic flows. This unit is finally overlain by K-poor, Mg-rich tholeiites. The regional scale folding of this belt, also manifested in the Chaibasa and Dhalbhum formations marker horizons, have E-W axial traces in the western and central parts and NE-SW axis in the eastern part. Further north of the Dalma belt and south of the CGC is a domain of pelitic and tuffaceous metasedimentary rocks having additionally abundant chert, black shale-chert rhythmites, acid volcanics and some syenitic rocks. Its northern margin with the CGC is marked by a brittle-ductile shear zone.

2.3. Chotanagpur Gneissic Complex (CGC)

The CGC lies with an overall east-west trend over parts of Uttar Pradesh, Madhya Pradesh, Bihar, Jharkhand and West Bengal and comprises largely of granitic and granitic gneiss bodies along with numerous enclaves of pelitic schists of varying compositions and grade of metamorphism, calc-silicates, marbles, quartzites, amphibolites, gabbro-norites, alkaline rocks, ultramafic rocks, anorthosite, charnockite, pyroxene granulite and skarn rocks. The meta sediments and majority of associated basic rocks have undergone metamorphism up to lower amphibolite facies. The granitic rocks have a compositional range from granite through granodiorite to tonalite. The occurrence of migmatites and gneisses are attributed to syn- to late kinematic partial melting with respect to peak

deformation and metamorphism conditions. The southern margin of the CGC has a brittle-ductile shear zone and carbonatite and alkaline rocks have been reported from this area (Ghosh Roy, 1989).

2.4. Singhbhum Shear Zone (SSZ)

The Singhbhum shear zone (also called copper belt thrust zone) 1-10 km wide and 200km long arcuate belt extending from Baharagora in east and Porahat in the west. Beyond Porahat it grades into high angle fault and extends up to western margin of Bonai granite. The shear zone is characterized by extreme ductile shearing, multiple metamorphism, migmatization and prominent mineralization in Cu, U, phosphate. The ductile shear zone consists of granite mylonite, quartz-mica phyllonite and quartz-tourmaline rock. The shear zone is often overlies Dhanjori formation and Koira group of rocks. Oligomictic sheared conglomerate intervein the shear zone. The normal order of superposition in the lithological sequence is followed on the either side of the shear zone, and here no structural, depositional break are found. But kyanite quartzite marked some transitional zone. During Dhanjori and Koira depositional cycle generate most of the pelites and volcanoclastics, which defines as the shear zone material. The shear zone is characterized by ultramafic intrusions such as hornblende schist, talc schist and serpentinite. Several detached felsic intrusive bodies like the Arkasani granite, granophyre, soda granite and feldspathic schists were formed due to shearing event. Repeated phases of folding, mylonitisation and rotation of fabrics marked the deformation history of shear zone. The sense of shearing show uniformly reverse or up dip movement during thrusting. The structural evolution is related to N-S to NNE-SSW subhorizontal compression, superposed by strong shearing movement in the south and west. The evolution of singhbhum shear zone is multi-episodic (Misra, 2006) at 2200 Ma, 1800 Ma, 1600 Ma and 1000 Ma.

2.2 Local Geology

In Pathargora (22° 32' 32.1 " N 86° 26' 22.4" E) area several kinds of rocks are there. Feldspathic schist, chlorite--biotite schist, apatite-magnetite pocket which are hosted by feldspathic schist. In general, however, the rocks in and around Pathargora are represented mainly by Singhbhum group of meta-sedimentary rocks. The litho-types belonging to Chaibasa Formation of Singhbhum Group of meta-sediments are represented mainly by polymictic conglomerate, quartzite, quartz-sericite schist, quartz-chlorite/chlorite-quartz schist, quartz-chlorite-sericite schist, quartz- tourmaline-rock (tourmalinite), pyrophyllite-rich sericite-quartz schist and feldspathic schist/gneiss. The meta- sedimentary rocks overlie the Singhbhum Granite exposed on the south-west of Pathargora. Singhbhum granite (22°43'21.1"N/ 86°00'43.6"E) composed of predominantly of quartz, feldspar and. The rock is coarse-grained and nearly massive in nature, with weakly developed foliation at places but interlocking texture can still be identified.

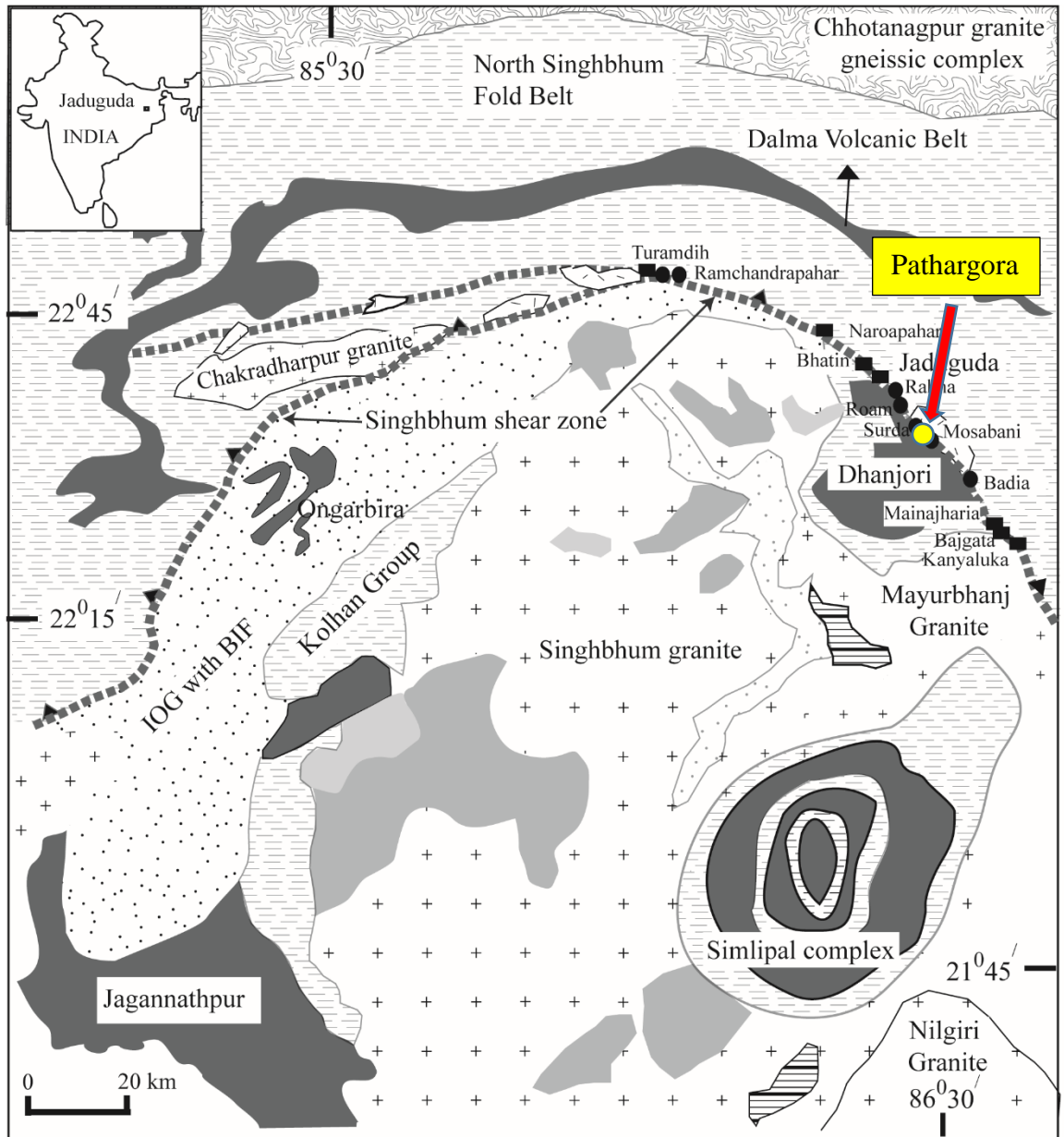
Quartzite exposed in Pathargora is mineralogically and texturally diverse. In both the areas quartzite occurs as small hillock. Near pathargora quartzite shows slickenslide surface where mineral lineation has developed. It is occurring close to the feldspathic Schist (mentioned above). Quartzite belonging to Chaibasa formation are laterally impersistent. Some of these quartzites are nearly massive in character, while some are distinctly banded with alternating quartz-rich and magnetite-rich bands. In both the areas conjugate fracture have been seen. Schistosity is prominent in micaceous-quartzite, containing sericite.

Feldspathic schist is mainly schistose in nature but weakly developed alternative bands of dark coloured and light coloured minerals are present. Light coloured band is defined by mainly quartz and kaolinite, albite, sericite (secondary alteration of muscovite) and minor apatite. Dark coloured band is defined by mainly biotite (80%), magnetite and sparse fine grained tourmaline. Chlorite is also present within the dark band but abundance is very low. Biotite is defining the schistosity. Tourmaline are present on the schistose plane with an extremely high abundance (near about 35%). Tourmalines are present on the alternative unites of schistose rock.

Chlorite-quartz schist or quartz-chlorite schist is melano-cratic, fine- to medium-grained schistose rock comprising variable proportions of quartz, chlorite, magnetite, apatite and sericite. Volume proportion of quartz and chlorite varies at different exposures of the rock. Thus may be termed as quartz-chlorite schist or chlorite-quartz schist depending on the most dominant mineral. The volume proportion of chlorite is ≤ 50 vol. percent of the rock. The prominent schistosity plane in

the rock is defined by chlorite grains. Prominent zones of silicification exemplified by foliation-parallel quartz veins are common. Additionally, quartz-tourmaline veins and quartz-chlorite veins are also present.

Tourmaline in the Pathargora area is coarser-grained compared. Quartz dominates over tourmaline in this rock and the rock appears more to be tourmaline-bearing quartzite. Additionally the rock is mineralogically heterogeneous and locally grades into reddish quartzo-feldspathic mass containing much less tourmaline. Somewhere massive very fine grained tourmaline rich bands are present within the quartz-tourmaline rock quartzite which may not be of same generation of original quartz-tourmaline country rock. In some cases these layers are associated with some quartz veins which cut across the original quartz-tourmaline fabric. Later quartz veins further cut across the fine grained tourmaline layer which in this case is more or less parallel to overall banding. Secondary copper minerals i.e; malachite are present as patches at some places. Chlorite-quartz-sericite schist appears to be one of the most extensive rock types in the area. However, due to the low preservation potential they are mostly soil covered and reasonably large exposures are present only when this rock is silicified, exemplified in the form of quartz veins.



LEGEND

- Older Metamorphic Group (Supra-crustals)
- Older Metamorphic Tonalitic Gneiss (OMTG)
- Iron Ore Group (IOG) greenstone sequence with BIF
- Granitoids
- Ultramafic intrusives

- Volcanic sequence
- Sedimentary sequence
- Feldspathic schist
- Singhbhum shear zone

Deposit locations

- Uranium
- Copper

Fig 2.1. Geological map of the Eastern Indian Shield. Yellow point indicates the study area (Pathargora) (Modified after Saha, 1994)

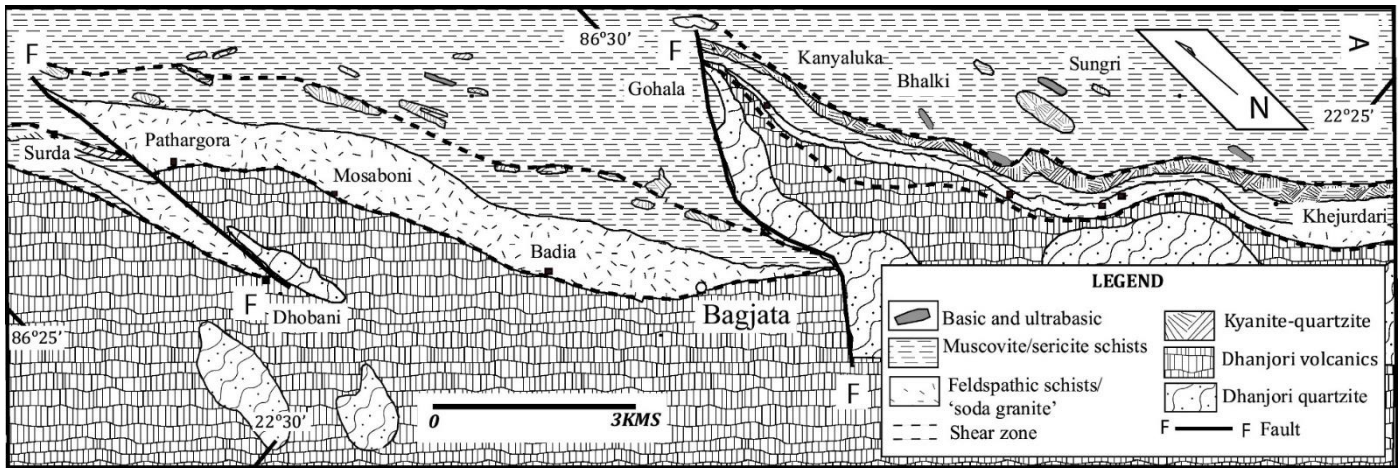


Fig 2.2: Lithological map showing the distribution of different rock types in and around the Pathargora (adopted from Talapatra, 1968).

Chapter 3: Description of host rock, mode of occurrence and texture of ore minerals

3.1 Introduction:

In this chapter, the host rock of different ore mineral phases and the mode of occurrence and texture of the ore minerals are described and documented. Hand specimens were initially studied in the field and in the laboratory. This was followed by petrographic study using optical microscope and scanning electron microscope (SEM) for further detailing.

There are two different associations in which magnetite occur:

- ❖ Magnetite-apatite ore comprising magnetite + apatite \pm biotite \pm quartz (M1)
- ❖ Magnetite-ilmenite ore comprising magnetite + ilmenite \pm apatite (M2)
- ❖

3.2 Magnetite-Apatite bearing feldspathic schist:

• Field Description:

The host or country rock is highly foliated schistose rock (Fig 3.1 a). The specific gravity is low. The rock comprises predominantly of albite, quartz, chlorite and sericite with varying proportions of kaolinite (altered from feldspar). The name of the rock is feldspathic schist (Fig 3.1a,b). The rock is almost devoid of biotite. However, there are biotite-rich zones in this feldspathic schist, often characterized by massive biotite (Fig 3.1 c). These biotite rich zone show concordant relationship with the host rock. Within the biotite-rich domain coarse grains of disseminated biotite porphyroclasts are wrapped by fine grained biotite grains with a preferred orientation (Fig 3.2f). Other minerals present in the biotite-rich portion are disseminated magnetite and apatite (Fig 3.1e). Some disseminated pyrite grains are also present but the abundance is very low (Fig 3.1 c).

Schistosity defined by feldspathic schist and biotite rich zone is concentrated along the is parallel and continuous (Fig 3.1 b). Attitude of foliation plane is $345^{\circ}/42^{\circ} \rightarrow E$.

There is small quartz tourmaline bearing veins and pockets, which show small scale pinch and swell structure. Magnetite-apatite veins of are present in the feldspathic schist. (Fig 3.1 b, d). These veins/pockets contain varying proportion of magnetite, apatite and biotite (Fig 3.1d) and are commonly surrounded by foliated biotite-rich zones (Fig 3.1b). The core of the apatite-magnetite veins is characterized by coarser grain relative to the boundary of the vein. These magnetite of apatite-magnetite vein associated with biotite is marked as M1a.

In contrast, there are some apatite-magnetite vein which are devoid of biotite grains ((Fig 3.4 d). These veins show asymmetric to sheath fold perpendicular to foliation plane of feldspathic schist. General trend of these veins are E-W. The width of the adjacent asymmetric magnetite-apatite vein (xz section) is 7cm (Fig 3.4 a). These magnetite of apatite-magnetite is marked as M1b.

- **Study of thin section under Optical microscope and Scanning Electron Microscope (SEM):**

Nine polished thin sections from this region were studied under optical microscope and scanning electron microscope for further detailed study.

There are some veins which shows zoning of apatite and magnetite band. In magnetite zone, magnetite size ranges from coarse to moderately coarse (150-400 μm). These grains are less fractured and less oxidized (Fig 3.3 d-BSE image). In apatite rich zone, apatite shows bimodal size distribution where coarse grains are subhedral to anhedral and some of them show hexagonal shape (Fig 3.2 b). These coarse grains are highly fractured. Fractures are filled with biotite-quartz-magnetite-hematite. Coarse apatite grains contain euhedral to subhedral magnetite inclusions (Fig 3.2e). Inclusions of monazites are present in apatite grains (Fig 3.2d). Monazite inclusions are clustered in coarse grained apatite. In some case monazite grains are less dense in the rim of the grains (Fig 3.2d) (mostly for hexagonal shape). These monazite grains do not show any preferred orientation in host apatite. Xenotime grains are also included in apatite. Monazite and xenotime phases have a very bright appearance in back scattered electron images (BSE). Number of

inclusions is less in elongated grains (Fig 3.2d). Some euhedral to subhedral, finer fraction of magnetite grains associated with anhedral to subhedral biotite grains are present in the intergranular spaces of apatite grains (Fig 3.2b, c). Biotite grains of this kind are haphazardly oriented (Fig 3.3a). Lath shaped ilmenite are associated with biotite grains. The magnetite grains associated with biotite in the intergranular zone of apatite are relatively more oxidized than the magnetite rich zone. These magnetite grains are isolated. An alternative band of lighter quartzo-feldspathic band and darker part of biotite-chlorite band surround the whole zone spatially (Fig 3.2 c). Disseminated very fine grained magnetites (60-100 μm) are present within these alternative bands (Fig 3.2 c). Quartz grains are mostly anhedral showing undulose extinction (Fig 3.2d)

Overall there are two modes of occurrences of magnetite-

1. Magnetite cluster in which coarse magnetite grains are less oxidized
2. Disseminated highly oxidized moderately coarse to fine magnetite grains are occupying the intergranular spaces of apatite and as well as associated with the feldspathic schist.

These magnetites from apatite-magnetite vein are M1a type magnetite.

In the magnetite-apatite vein sample, magnetite grains are ranging from very fine grained (50-60 μm) to coarse grained (300-400 μm) (Fig 3.7e,f). In the contact zone of apatite-magnetite, magnetite grains are very fine grained (Fig 3.7 e). Ilmenite is associated with this part. Whereas apatite grains are very coarse and inclusion rich. The pattern of inclusion rich zone differs from grain to grain. These magnetites of magnetite-apatite are M1b type which contains no biotite.

3.3 Magnetite-ilmenite \pm apatite-bearing host feldspathic schist:

• Field Description:

The host rock is highly sheared and shows extensive foliation. This is noted as ultramylonitic zone. The host rock is feldspathic schist but it has comparatively more biotite and chlorite than the apatite-magnetite host rock (Fig 3.3 e,f). There is a massive pocket of magnetite body in the southern part of shear zone which is mostly devoid of apatite (Fig 3.4a). Large mica (biotite) books

are associated with magnetite body (Fig 3.4b,c). Quartz vein is also present in this body. Attitude of foliation plane is $340^{\circ}/40^{\circ}\rightarrow\text{NE}$.

Fold axis lineation data is $20^{\circ}\rightarrow 103^{\circ}$.

Maximum length of magnetite body is 90cm and maximum height of body is 120cm (measured at xy plane, parallel to foliation plane). Samples from the magnetite body are collected from the boundaries and the central part.

• Study of thin section under Optical microscope and Scanning Electron Microscope (SEM):

Magnetite grains from massive magnetite body are very coarse and oxidized in varying degree. Different ilmenite grains are embedded within host magnetite grains and possess different types of relationship with host magnetite grains. Absences of ilmenite grains are noted in some magnetite (Fig 3.5 b). Some of the magnetite grains are highly fractured. Biotite, quartz and fine grained elongated ilmenite grains fill the fracture zone (Fig 3.4 e,f, Fig 3.6 b). Biotite grains are haphazardly oriented within these fractures. Very few amount of apatite grains fill the fracture.

The magnetite associated with ilmenite lamellae are defined as M2a. Whereas, the magnetite hosted very few to no ilmenite lamellae are marked as M2b.

Based on the ilmenite exsolution morphology and texture, they are divided into 4 types:

1. **Thin lamellar type-** These type of exsolutions are very fine ($<1\text{-}10\mu\text{m}$) in nature. They are mostly oriented along one dominant set of $\{111\}$ planes of magnetite host and densely crowded. (Fig 3.5e). $\{111\}$ planes of spinel and $\{0001\}$ plane of ilmenite is structurally similar which accounts for the common orientation of fine ilmenite exsolution. These lamella show sharp contact with their magnetite host. They have more or less uniform width throughout a single grain of magnetite. In some cases, they are fused with their immediate neighbors to form lath shaped wider lamellae ($10\text{-}30\mu\text{m}$).
2. **Sandwich type-** Thick ilmenite lamellae predominantly in one set of $\{111\}$ planes showing preferred orientation. The thickness/width of these thick ilmenite lamellae vary from 25 to

90 μm . The boundaries are mostly sharp and regular (Fig 3.6c). Very few boundaries are irregular (Fig 3.5e) and discontinuous. Some thin/thick ilmenite lamellae contain patches of ilmenite which have different crystallographic orientation with respect to host ilmenite lamellae as it can be seen by different pleochroism. Sandwich type exsolution shows bifurcation in places. Sandwich types of laths are coexisting with thin lamellae type and composite type, though they are rarely in contact (Fig 3.5 e).

3. **Composite type-** - These are irregular patchy ilmenite granules within host magnetite (nearly pure and hematitized) without any preferred orientation. In some cases, they continue to more or less lamellae type ilmenite exsolution. (Fig 3.5e)
4. **Net texture-** Thin ilmenite lamellae (predominantly have a general orientation as sandwich type lamellae) are interconnected to adjoining relatively thicker ilmenite lamella forming net type texture . The interstitial spaces are occupied by host magnetite (Fig 3.6c)

Except this, ilmenite lamellae are typically concentrated along cracks (Fig 3.5 a), around silicate inclusions, and, most significantly of all, along magnetite grain boundaries. ilmenite in these oxidized lamellar zones increases in size and abundance towards the grain boundaries. As they approach towards center of the host grain, they taper. There are recrystallized ilmenite grains which rimmed magnetite grains. These ilmenite grains are subhedral to euhedral in shape. These grains also contain very less amount of Fe- rich exsolution. Xenotime is associated with these types of ilmenite grains. (Fig 3.7 a,b)

There are some irregular shaped ilmenite grain which contain different shaped (oval, granular, straight) Fe-rich exsolutions. These types of exsolutions are mostly concentrated in the core part of the grain and rim part is completely devoid of these types of exsolutions (Fig 3.6a).

Some of the exsolution lamellas of ilmenites are sheared within magnetite host and bended in nature. (Fig 3.6a,c).

Some relatively finer magnetite grains are crosscutting thick lamellar ilmenite exsolution (Fig 3.5c).

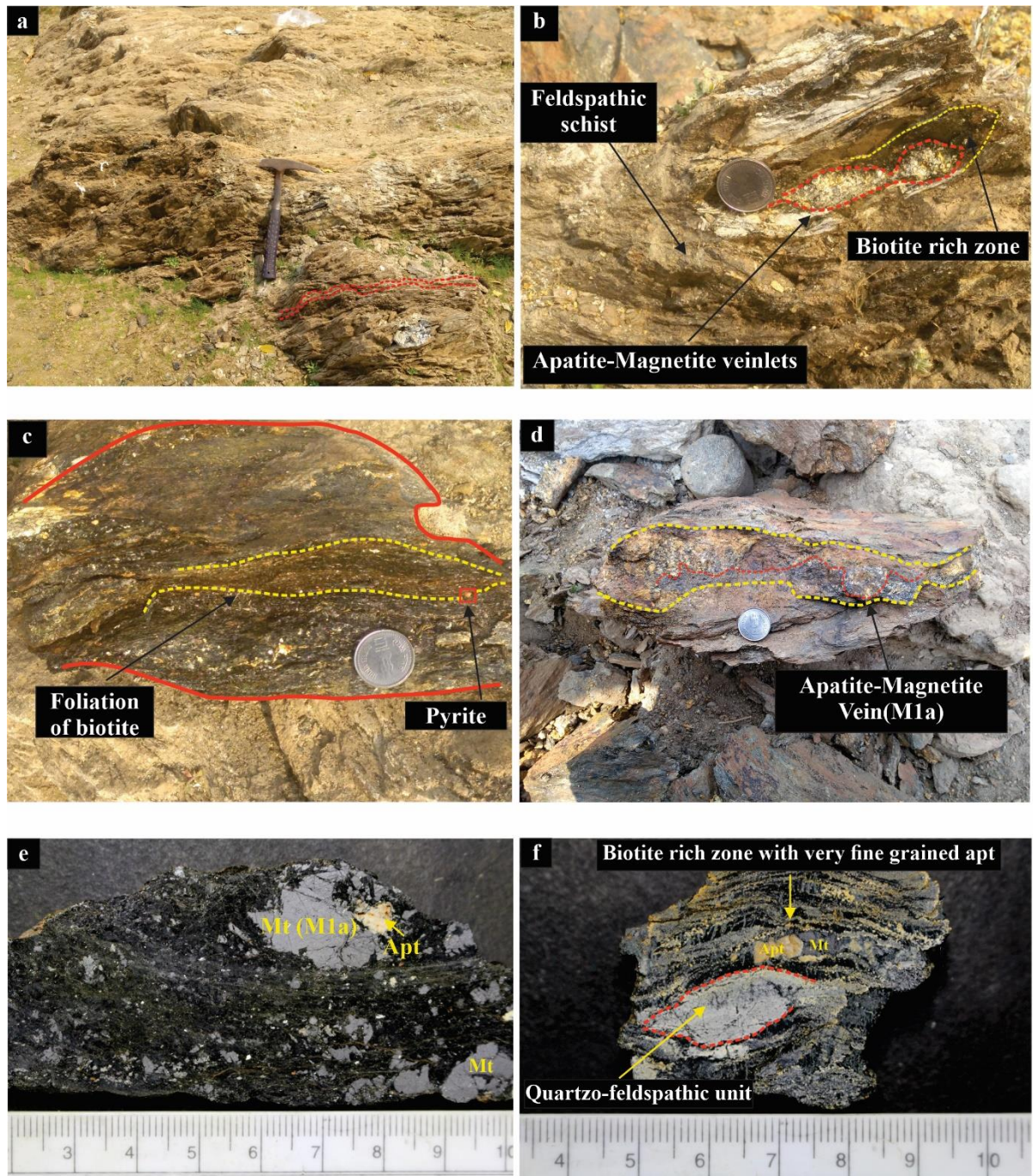


Fig 3.1: Field (a) and hand specimen (b, c, d, e, f) photograph of different rock types, (a) schistosity (marked with dotted red lines) defined by feldspathic schist, (b) biotite rich zone (yellow marker) in feldspathic schist; apatite-magnetite veins are present within biotite rich zone, (c) biotite defined by red solid line, and disseminated pyrite grains, (d) varying proportion of apatite-magnetite in vein; apatite rich zone in the upper part and magnetite rich zone in the lower part, separated by red dotted line, (e) magnetite (coarse to disseminated finer grains in the lower part) and very less proportion apatite are embedded within biotite rich zone, (f) magnetite-apatite is surrounded by biotite, alternative biotite-rich and quartzo-feldspathic zone and a pocket of host rock (marked by red dotted lines) is wrapped by biotite. Abbreviations: Mt- Magnetite, Bt- Biotite, Apt-

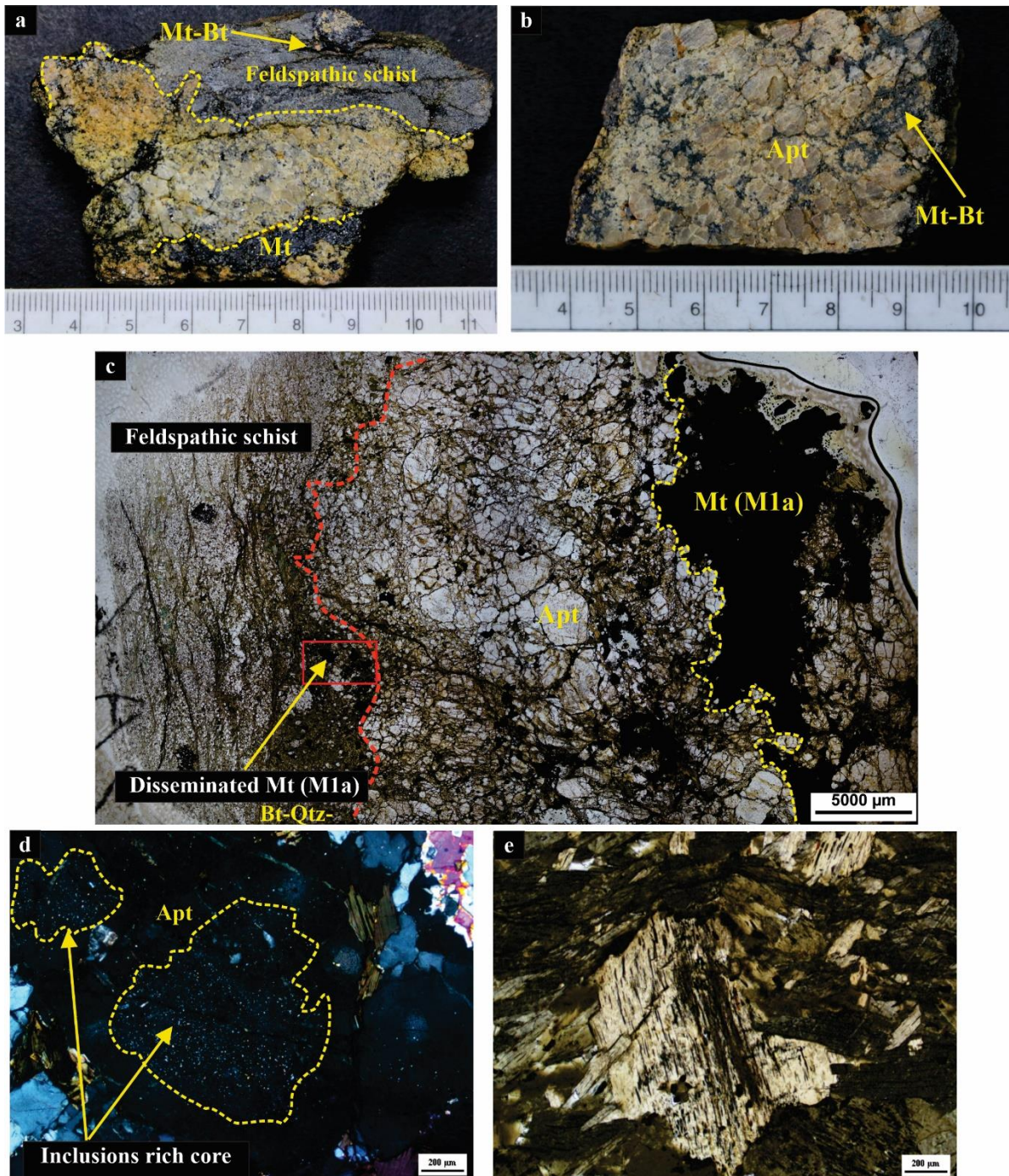


Fig 3.2: Hand specimen photograph (a, b) and microphotographs (c, d, e) of different rock types, (a) magnetite rich zone (lower part) is separated from light coloured apatite rich zone; feldspathic schist is intervened by biotite-magnetite, (b) section of apatite-magnetite vein; darker magnetite-biotite filled the intergranular zone of coarser apatite, (c) microphotograph of image (a)- apatite rich zone in the middle bounded by magnetite rich zone in the right (yellow dotted marker) and feldspathic schist with biotite rich zone (red dotted line); disseminated magnetite are present in apatite rich zone and host rock, (d) Inclusions of monazite and xenotime in the core of apatite, (e) biotite porphyroclast is wrapped by finer and elongated biotite grain. *Abbreviations: Mt- Magnetite, Bt-Biotite, Apt-Apatite*

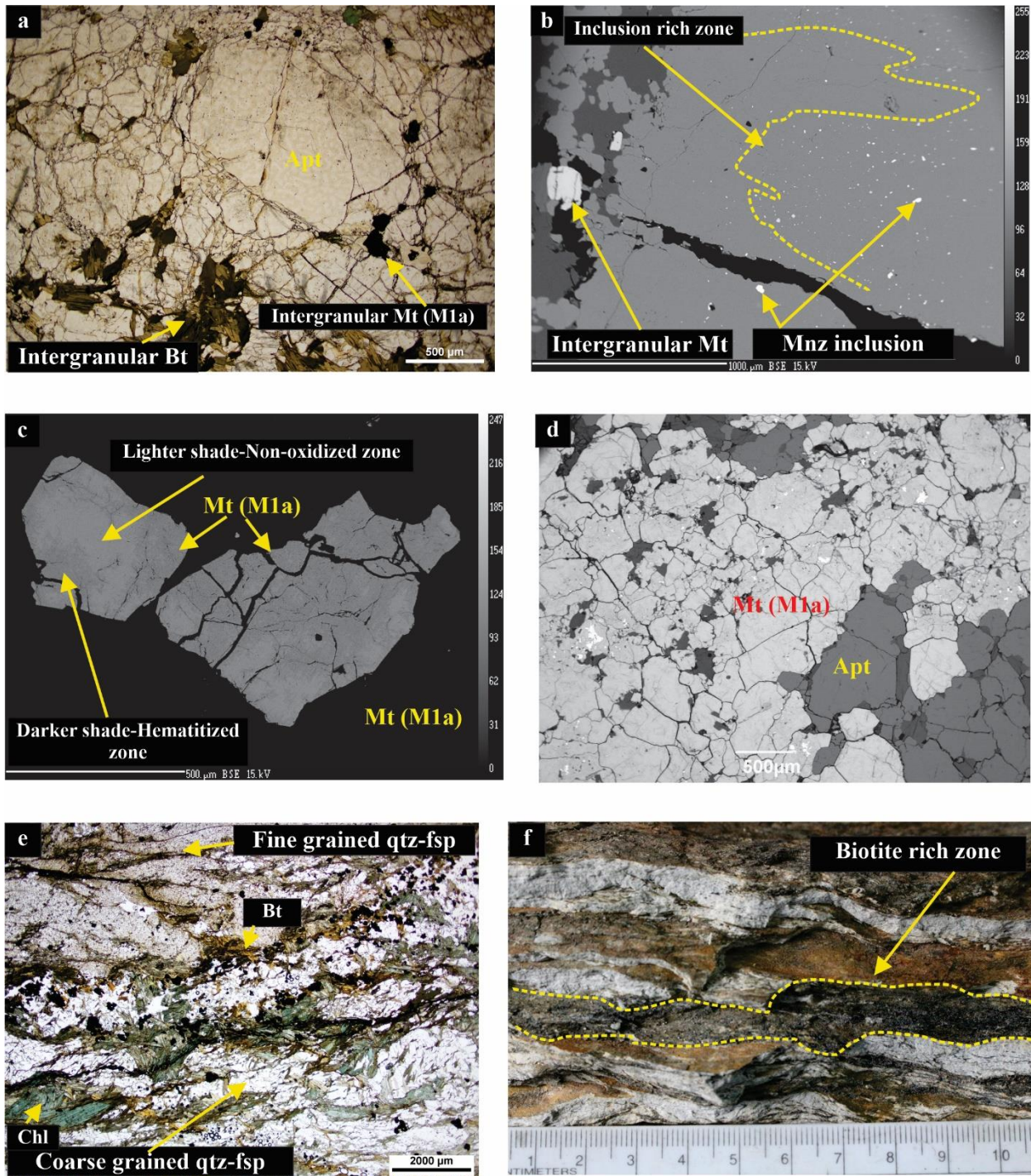


Fig 3.3: Hand specimen (f), microphotographs (a, e) and BSE images (b, c, d) of different rock types, (a) intergranular zones of apatite are filled with magnetite and haphazardly oriented biotite grains (left-lower part); biotite grains are associated with finer apatite, (b) inclusion rich zone in right is separated by yellow dotted line by inclusion free zone in the right, (c) highly fractured magnetite showing oxidized zone in the vicinity of fracture (darker shade) and non-oxidized zone (lighter shade), (d) relatively less oxidized highly fractured magnetite grains in magnetite rich zone, (e) coarse grained and fine grained quartzo-feldspathic band separated by biotite-chlorite rich zone, (f) biotite rich zone parallel to host rock. *Abbreviation: Mt-Magnetite, Bt-Biotite, Apt-Apatite, Mnz-Monazite, Chl- Chlorite*

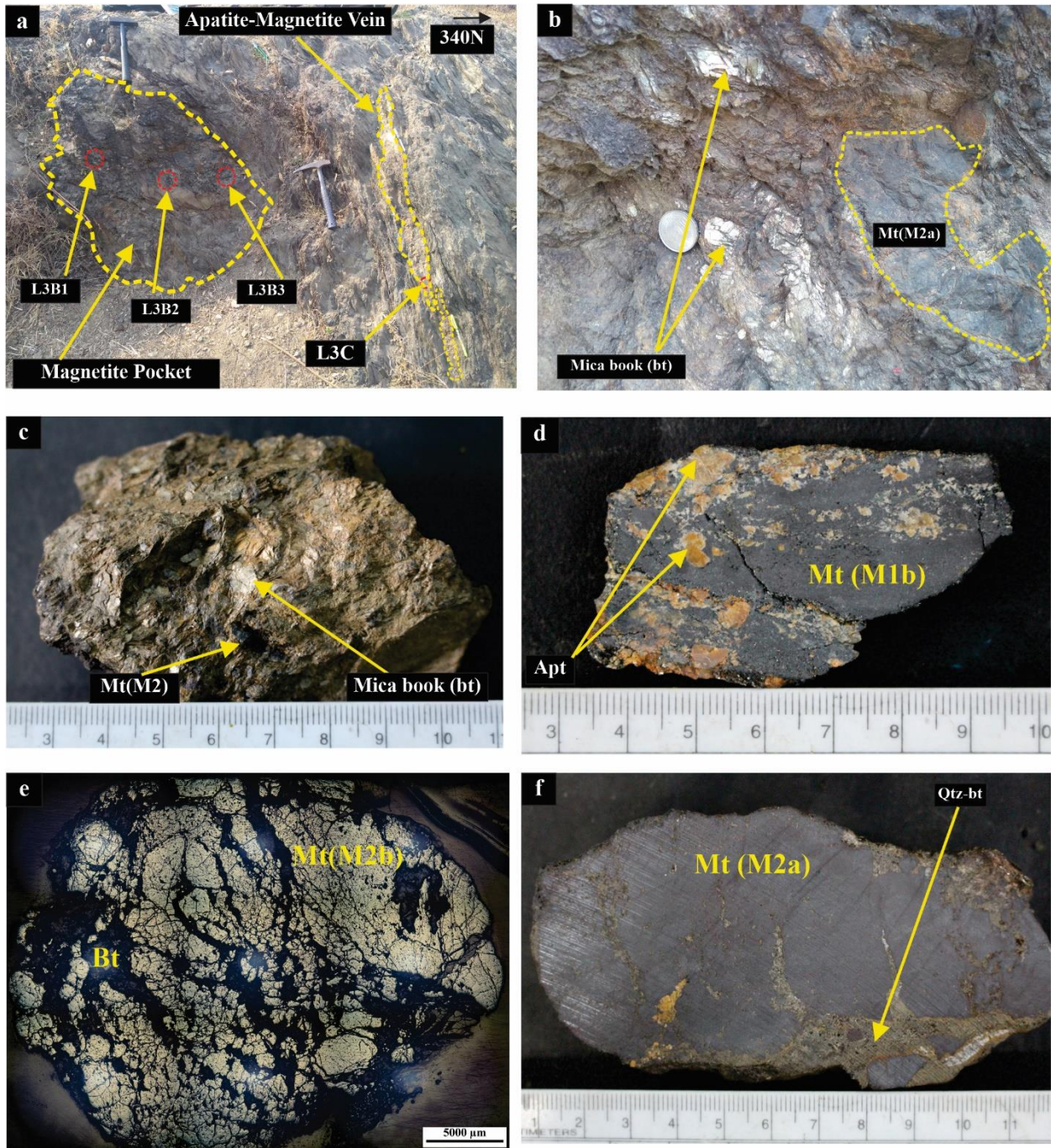


Fig 3.4: Field photograph (a, b), hand specimen photograph (c, d, f) and microphotographs (e) of different rock types; (a) massive magnetite pocket (M2) and sample locations are located, linear apatite-magnetite veins (M1b) are cross-cutting the foliation plane (in the right side of the image), (b) mica books (bt) are associated with magnetite grains, (c) mica books defined by biotite are associated with magnetite grains, (d) apatite-magnetite vein which is completely devoid of biotite, (e) intergranular spaces of magnetite grains filled by biotite, (f) fractures in magnetite are filled by quartz and biotite grains. *Abbreviations: Mt- Magnetite, Bt-Biotite, Apt-Apatite*

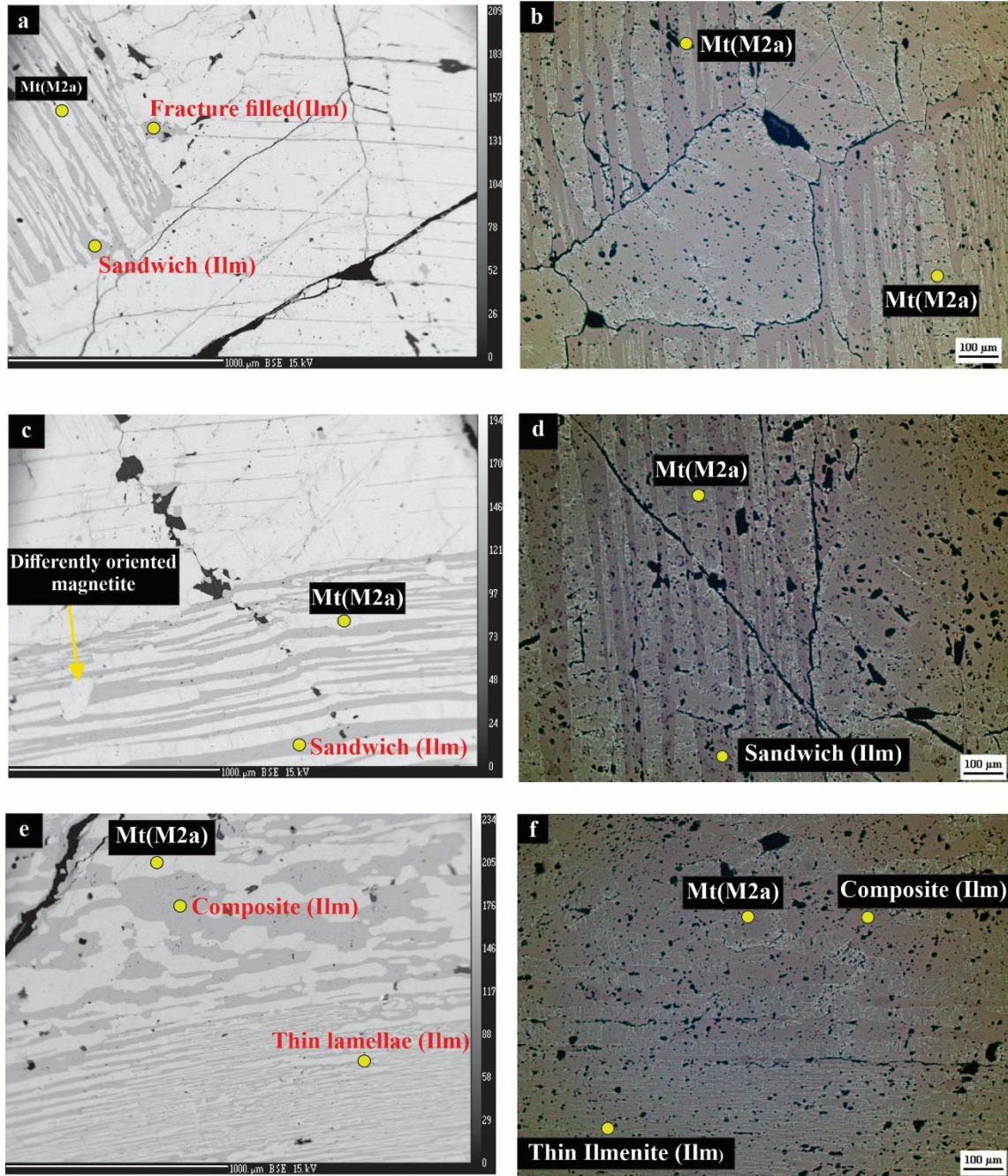


Fig 3.5. BSE images (a,c,e) and reflected light microphotographs (b,d,f) of different ilmenite hosted in magnetite, (a) isolated lamellar ilmenite exsolution; exsolution lamellae are coagulated near the fracture; the other part is pure magnetite with sparse thin ilmenite lamellae; irregular shaped ilmenite grains are concentrated along the cracks, (b) ilmenite free zone (top right to left bottom) separating the ilmenite exsolved zone, (c) thin lamellae to thick sandwich type ilmenite exsolution upper part is pure magnetite with sparse thin ilmenite exsolution, (d) thin lamellae to thick sandwich type ilmenite exsolution, (e) uniform width of ilmenite exsolution in the middle part of the image; composite type (irregular, patchy grain without preferred orientation) of ilmenite at the upper part of the image; lower part is mostly sandwich type lamellae with irregular boundary. Fine magnetite grain crosscutting ilmenite lamellae (f) optical image of fig e. Abbreviation: Mt-Magnetite, Ilm- Ilmenite

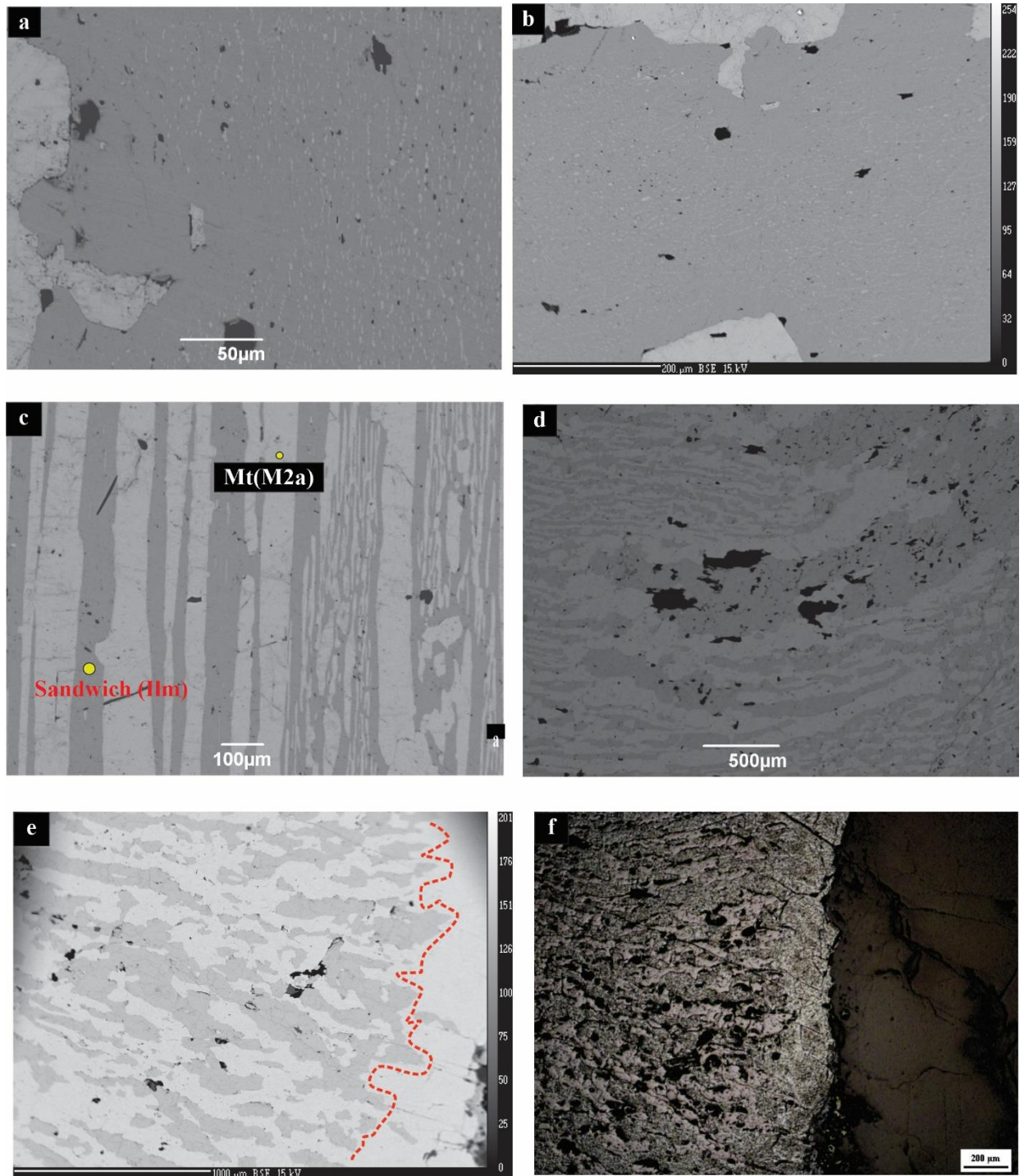


Fig 3.6. BSE images (a, b, c, d, e) and reflected light microphotographs (f) of different ilmenite hosted magnetite, (a) different shaped (granule, oval, oriented lamellar) Fe-rich exsolution (brighter phase) are hosted in the core part of ilmenite grain; rim part is devoid of these type of exsolution, (b) Fe rich exsolution in ilmenite, (c) sandwich type ilmenite exsolution show sharp contact with host magnetite (middle to left side), (d) composite type of ilmenite grain (top right to middle) which is continued to thin bended lamellae, (e) ilmenite rich part (right) is separated from oxidized zone in left by red dotted line, (f) optical image of fig e. Abbreviation: *Ilm*-Ilmenite, *Mt*- Magnetite

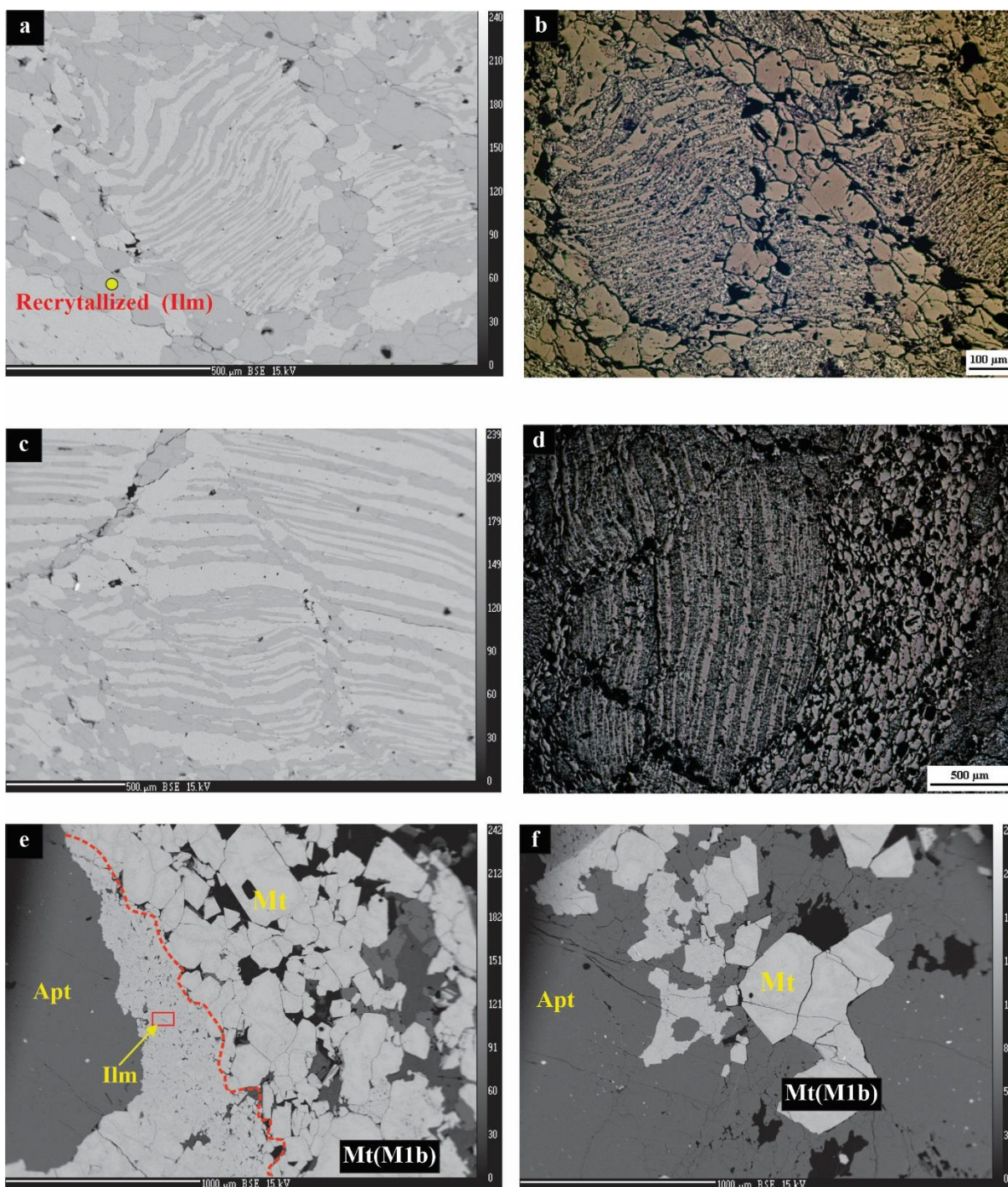


Fig 3.7. BSE images (a,c,e,f) and reflected light microphotographs (b,d) of different ilmenite hosted magnetite, (a) thin to thick sandwiched ilmenite lamellae are micro folded within magnetite host grain; recrystallized subhedral to euhedral grains rim the magnetite grain; brighter phase at the left part is recognized as Yt-phosphate, (b) optical image of fig a, (c) folded lamellae (left-right trend) intervened by ilmenite rich fracture zone (upper to lower, middle upper to right end), (d) aggregates of ilmenite grain at the left part of magnetite, (e) fine grained magnetite zone in the vicinity of apatite grain separated from coarse grained magnetite (M1b) (right) by red dotted line, (f) corrugated boundary of magnetite in intergranular spaces of apatite. *Abbreviation: Mt-Magnetite, Apt- Apatite, Ilm-Ilmenite*

Chapter 4: Geochemistry of Magnetite

4.1 Introduction:

In the previous chapter, the mode of occurrences of magnetite and their associated phases are discussed and documented. The various texture and relationship of magnetite, apatite and ilmenite are established in the field followed by further detailed characterization using optical microscope and scanning electron microscope (SEM). This chapter deals with detail major element geochemistry of magnetite and ilmenite.

4.2 Methodology and Analytical Procedure:

The geochemical analysis of magnetite and associated phases are done in three stages. The mineral phases are initially identified by semi-quantitative data generated from a JEOL JSM 6490 Scanning Electron Microscope (SEM) . Back scattered electron (BSE) images are obtained using the same SEM for better understanding of textures and intra-grain compositional variations.

For obtaining precise major element geochemistry Electron Microprobe Analyzer (EPMA) is used. Magnetite composition were determined on polished carbon coated thin section by a Cameca SX-100 EPMA equipped with four wavelength dispersive spectrometers (WDS). This was operated at acceleration voltage of 15 kV, beam current of 20nA and beam size of 5 μ m.

All the analysis were performed at the Department of Geology and Geophysics, Indian Institute of Technology (IIT), Kharagpur.

4.3 Mineralogy of Magnetite and Ilmenite:

Magnetite (Fe_3O_4) is an important petrogenetic indicator and pathfinder mineral with a wide array of applications including geophysical studies, igneous petrology, provenance studies and mineral exploration (e.g., Dupuis and Beaudoin, 2011; Ghiorso and Sack, 1991; Grant, 1984-85; Lindsley, 1976; McClenaghan, 2005; Razjigaeva and Naumova, 1992). Magnetite has an inverse spinel structure with the general stoichiometry XY_2O_4 , where the X or octahedral site is occupied by divalent cations such as Mg, Fe^{2+} , Ni, Mn, Co, or Zn, and Y or tetrahedral site is occupied by trivalent cations such as Al, Fe^{3+} , Cr, V, Mn, or Ga (Lindsley, 1976; Wechsler et al., 1984). Depending on the environment various types of minor and trace elements are incorporated into these two sites. Ti^{4+} can also occupy the Y site when substitution is coupled with a divalent cation (Wechsler et al., 1984) at X site. Subequal numbers of ferric (Fe^{3+}) and ferrous (Fe^{2+}) iron atoms randomly occupy the octahedral site, whereas tetrahedral sites are exclusively occupied by the smaller ferric iron atoms $\text{Fe}^{3+}[\text{Fe}^{2+}\text{Fe}^{3+}]\text{O}_4$ (Lindsley, 1976; Waychunas, 1991; Wechsler et al., 1984).

Ilmenite commonly shows intergrowth with magnetite and hematite. Ilmenite is an iron-oxide mineral with structural formula FeTiO_3 . Fe^{2+} and Ti^{4+} ions are both in octahedral co-ordination. It contains significant amount of Mg^{2+} and Mn^{2+} for both Fe^{2+} .

4.4 Major Element Geochemistry of Magnetite:

In this section, the geochemical composition of the various mode of occurrences of magnetite is described. Major oxide percentages are converted into atoms per formula unit (a.p.f.u) based on 32 anions and 24 cations.

a. Apatite-Magnetite vein (M1):

These types of magnetite grains are extensively oxidized. It has been mentioned in the previous chapter that in some apatite-magnetite vein biotite is ubiquitous whereas in another variety biotite is absent. The magnetite grains associated with biotite and those which are devoid of biotite are henceforth defined as M1a and M1b respectively for the ease of discussion. The M1a and M1b are

indistinguishable from each other in terms of their major element compositions although they have substantial difference in trace element compositions (Chapter 5). The Na_2O , CaO , TiO_2 , Cr_2O_3 , SiO_2 and MnO concentration are below detection limit in both these varieties. The MgO content varies between 0.03 and 0.18 wt% with an average value of 0.04 wt% (Fig 4e). Al_2O_3 concentration ranges from below detection limit to 0.27 wt% (Fig 4e). V_2O_3 concentration is low and varies from 0.25-0.45 wt% (Fig 4a). Total FeO is recalculated to obtain Fe_2O_3 and FeO weight percentage separately. The calculated values range from 62.09-70.79 wt% and 29.47-32.05 wt% for Fe_2O_3 and FeO respectively (Fig 4f).

b. Massive Magnetite body associated with Ilmenite (M2):

It has been mentioned in the previous chapter that in the massive magnetite body some magnetite contains ilmenite exsolution whereas some others are devoid of any such exsolution. In the following discussion those with ilmenite exsolution and those which are devoid of ilmenite exsolution are referred to as M2a and M2b respectively. In comparison to M1 magnetites in apatite-magnetite vein, magnetite associated with ilmenite (M2a) shows relatively high concentration of V_2O_3 and Cr_2O_3 (Fig 4 a,b). The V_2O_3 content ranges from 0.70-0.98 wt% whereas Cr_2O_3 varies from below detection limit to 0.66 wt%. Average concentration of MgO in magnetite is 0.05 wt% with the highest concentration being 0.08 wt% (Fig 4e). Al_2O_3 content ranges from 0.06 wt% to 0.75 wt% with an average concentration of 0.18 wt% (Fig 4e). The M2a and M2b magnetites are distinctly different in their TiO_2 contents. The TiO_2 content in M2b is mostly below detection limit. In contrast M2a magnetite that hosts ilmenite exsolution lamella has a higher concentration of TiO_2 with an average concentration of 0.18 wt% having maximum value of 0.8 wt% (Fig 4 a). Cr_2O_3 is also very low (0.08 wt%) in M2b and more or less similar to that in M1 magnetites (0.06 wt%) in apatite-magnetite vein (Fig 4b). The total FeO ranges from 86.05 wt% to 93.30 wt%. The calculated Fe_2O_3 and FeO ranges between 62.68 to 68.56 wt% and 29.47 to 32.05 wt% respectively. The Na_2O , CaO , MnO concentrations are mostly below detection limit in all M2 magnetites. Silicon is also mostly below detection barring the exceptions of some grains where the SiO_2 contents range between 0.21 to 0.26 wt%.

The MgO concentration in Ilmenite lamella ranges from 0.08 to 0.31 wt%. Irrespective of different shape and size and type of the exsolutions, TiO_2 concentration of ilmenite lamella ranges between 43.85 and 50.96 wt%, and FeO content ranges from 46.30 to 53.95 wt%. MnO concentration in

ilmenite lamella is comparatively higher than the host magnetite and ranges from 0.423 to 1.70 wt%. Al_2O_3 concentration is quite similar to that of the host magnetite and ranges in between 0.12-0.18 wt%. V_2O_3 concentration is very low with average value being 0.17 wt%. From the recalculated value of total FeO, FeO and Fe_2O_3 are showing 38.53-44.75 wt% and 2.39-7.00 wt% respectively. The Na_2O , CaO and Cr_2O_3 values are below detection limit in ilmenite exsolution lamella.

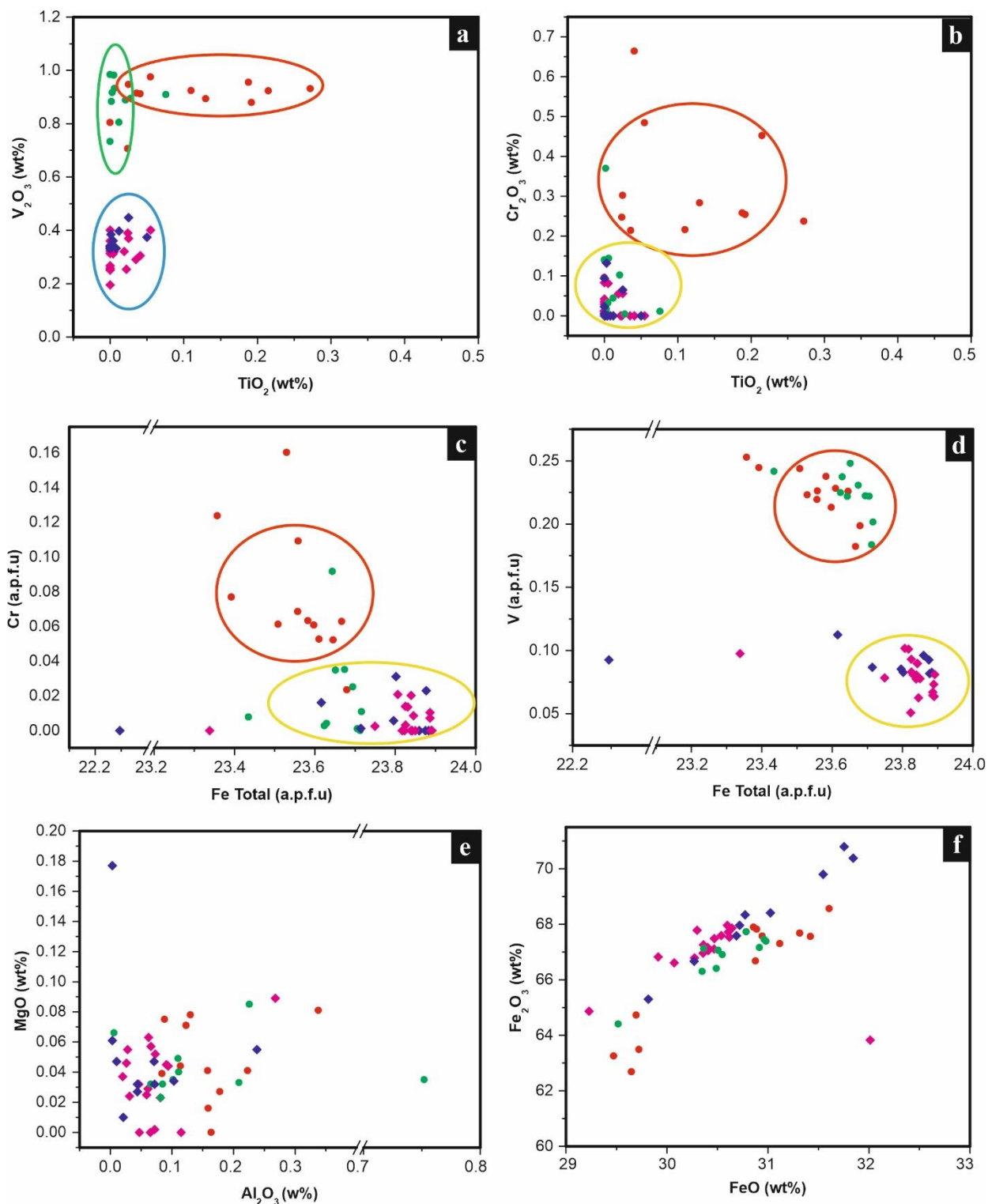
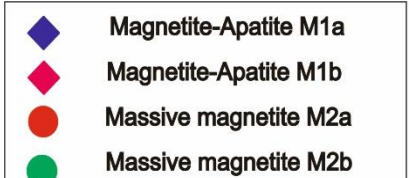


Fig 4: Binary plots showing the major element compositional variations in different types of magnetite



Chapter 5: Trace Element Geochemistry of Magnetite

5.1 Introduction:

Magnetite can incorporate a large number of minor and trace element in its structure depending on physicochemical parameter of the formation environment. Dare et al. (2014) measured the variable concentration of Mg, Al, Si, P, Ca, Sc, Ti, V, Cr, Mn, Co, Ni, Cu, Zn, Ga, Ge, Y, Zr, Nb, Mo, Sn, Hf, Ta, W and Pb in magnetite from different types of deposit using LA-ICP-MS.

5.2 Analytical Procedure:

The trace elements concentrations in minerals were measured using a Thermo Fisher Scientific iCap-Q Quadrupole Inductively Coupled Plasma Mass Spectrometer (LA-ICPMS) coupled with a New Wave Research 193nm Ar-F excimer laser ablation system at the Department of Geology and Geophysics, Indian Institute of Technology (IIT), Kharagpur. The laser was operated at 5 Hz repetition rate and ca. 5 J/cm² beam energy density. Spots size were 45–50 µm for sample and bracketing standards. The instrument was optimized for maximum sensitivity in low medium and high mass range using the NIST SRM 612 reference glass. The raw counts for each isotope were measured in the time resolve mode with 30 second of gas blank without laser firing and 45 second during ablation. The external standardization was done by bracketing the group of ten unknown with two measurement of the NIST SRM 610 glass. The data was reduced off line using the GLITTER © data reduction software. The data quality was monitored by analyzing the reference glass NIST SRM 612 as unknown interspersed with the measurements of the samples.

5.3 Trace element Geochemistry:

a. Apatite-Magnetite vein:

Similar to that of major element concentrations, the different magnetite show different trace element concentration. M1a and M1b, both magnetite in general have low concentration of spinel elements (Al, Ti, Mg, Mn, Zn, Cr, V, Co, Ga). However they can be distinctly discriminated based on Ga and Ni concentrations. Gallium concentration is higher (83-110 ppm) in M1b magnetite relative to M1a magnetite (50-72 ppm) (Fig 4.1 e, b) where as Ni concentration is higher in M1a magnetite (640-759 ppm) compared to M1b magnetite (398-562 ppm) (Fig 4.1c). Additionally, Co concentration is higher in M1a magnetite and ranges from 82 to 147 ppm in M1a magnetite whereas the Co concentration in M1b magnetite ranges between 45 and 81 ppm (Fig 5.1 c). The Ti (avg. 354ppm), V (1984-3341 ppm), and Cr (15-204 ppm) are very low in concentration relative to the M2 magnetites in massive magnetite body (Fig. 5.1a, b, d).

b. Massive Magnetite body:

Compared to M1 magnetites in apatite-magnetite vein, both M2a and M2b magnetites in massive magnetite are enriched in Cr (527-758 ppm) and V (5769-8484 ppm) and Ga(92-183 ppm). The M2a and M2b magnetite are discriminated in Ga vs V (Fig 5.1b) Co vs Ni (Fig 5.1c) and Cr vs Ti (Fig 5.1d) diagram where it is evident that M2a magnetites are more enriched in Ga, Ni and Cr compared to M1a magnetites; M2b magnetite contains low concentrations of Cr (9.6-1434 ppm), Ga (92-128 ppm), Ni (475-527 ppm) relative to M2a magnetite that contains higher concentration of Cr (707-4226 ppm), Ga (125-183 ppm), Ni (534-748 ppm) (Fig 5.1 b,c,d).

5.4 Discriminant Diagram :

- Ti (ppm) vs Ni/Cr (un-normalized) diagram is used to distinguish between magmatic and hydrothermal settings (Dare et al. 2014). In silicate magma, Ni and Cr behave as couple

element where Ni/Cr ratios are generally ≤ 1 . However, they are decoupled in hydrothermal solution resulting in higher Ni/Cr ratios due greater solubility of Ni compared to Cr (Dare et al. 2014) in such solution. Though in oxidizing condition Cr^{+6} is highly mobile (in solution, Cr^{+3} is two to four orders of magnitude more soluble than Ni in magmatic system (Watenphul et al, 2012,2013) which results in low Ni/Cr for magmatic/magmatic-hydrothermal magnetite. The M2a magnetites and all the M1 magnetites are well within the magmatic field and hydrothermal field (Fig 5.2a) respectively whereas the M2b magnetites straddle the boundary between magmatic and hydrothermal field.

- Ni/(Cr+Mn) wt% vs (Ti+V) wt% show well-defined fields of IOCG, Kiruna-type, porphyry Cu and Fe-Ti-V deposits (Dupuis and Beaudoin, 2011). The M2a magnetite are plotted close to the boundary between magmatic Fe-Ti-V field and porphyry field whereas M2b magnetite show a wide range falling in the field of porphyry and Kiruna type deposits and beyond along with M1 magnetites. The M1 magnetites fall in the field of Kiruna type deposits and some that has higher Ni content fall beyond the field of Kiruna type deposits (Fig 5.2 b).

5.5 Multielement Variation Diagram:

25 trace element are plotted in order of increasing compatibility in magnetite structure, using the compilation of experimental and empirical partition co-efficients between magnetite and silicate magma (Dare et al. 2014). Magnetite are normalized to bulk continental crust due to its close composition to silicate melt than primitive mantle. Data of bulk continental crust is taken from Rudnick and Gao 2003.

With respect to data from Dare et al. 2014, this study shows low concentration of HFSE such as Sc, Zr, Hf, Nb, Ta, Ti and Mn (Fig 5.3) in magnetite. Hydrothermal magnetite (M1a, M1b) are characterized by low concentration of Ti, V, Cr compared to that of magmatic magnetite (M2).

Trace element concentration of ilmenite is also normalized to bulk continental crust in this study. Irrespective of their different exsolution pattern, they show high HFSE and Mn concentration compared to magnetite. However, they are depleted in V, Ni, Cr, Co compared to magnetite (Fig 5.4 a,b)

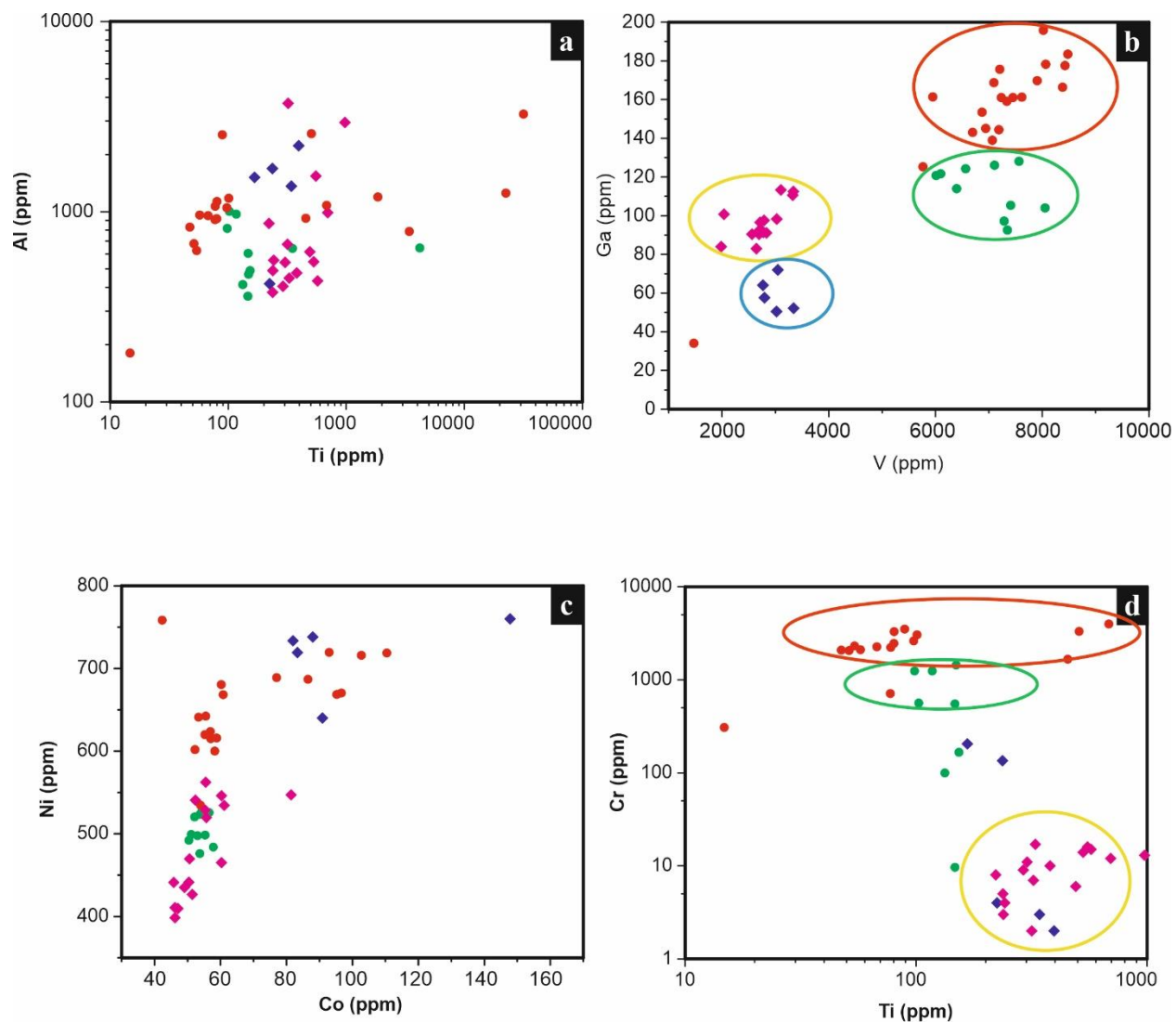
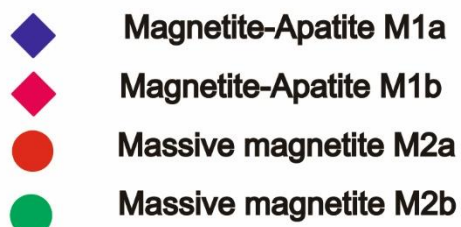


Fig 5.1: Binary plots showing differences in trace element contents of different magnetite types. (b) Showing the difference in Ga concentration for different types of magnetite (d) Difference in Cr concentration



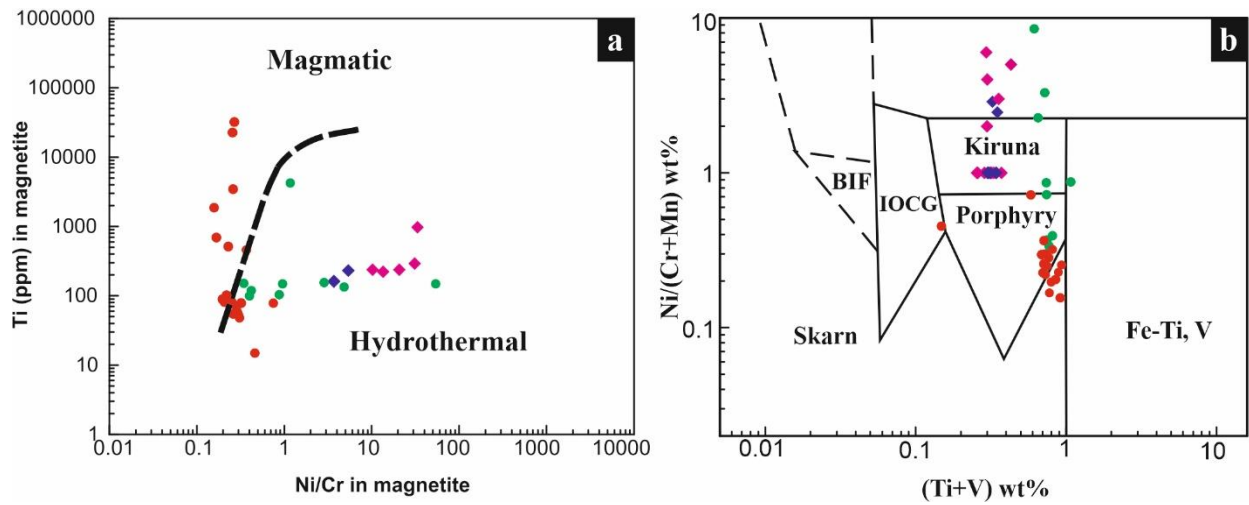


Fig 5.2: (a) Discriminant diagram for magmatic-hydrothermal after Dare et al. 2014 and (b) Discriminant diagram for average Fe-oxide compositions from Kiruna, IOCG, porphyry, Cu, Fe-Ti-V and BIF deposit after Dupuis and Beaudoin (2011)

- ◆ Magnetite-Apatite M1a
- ◆ Magnetite-Apatite M1b
- Massive magnetite M2a
- Massive magnetite M2b

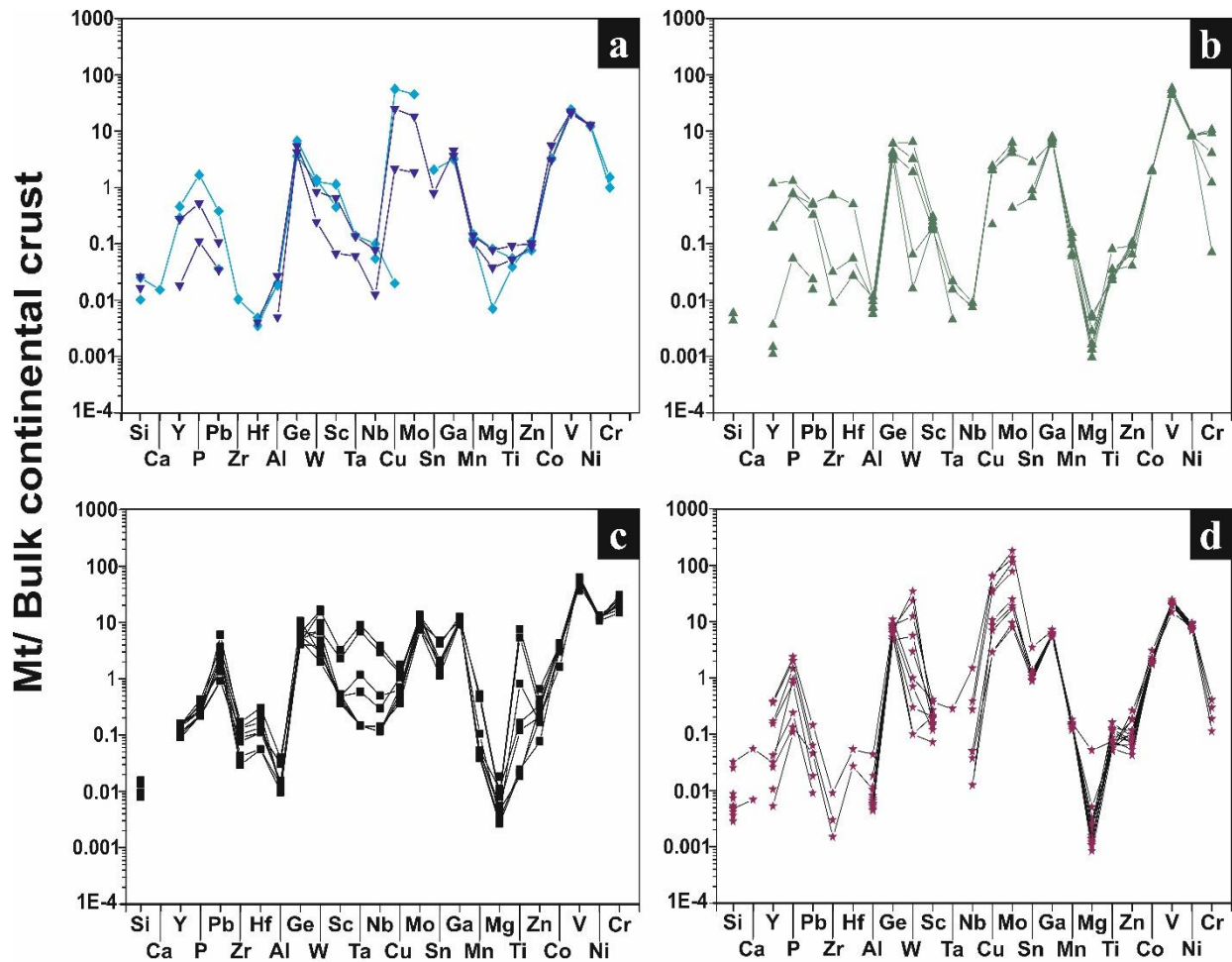


Fig 5.3: Multielement variation diagrams for magnetite (Mt) (Dare et al. 2014), normalized to bulk continental crust (values from Rudnick and Gao 2003). Compatibility of elements into magnetite are increasing from left to right. (a) M1a, hydrothermal magnetite contain low concentration of V, Ti, Cr; (b) M2b magnetite has variable concentrations of Ti, V and Cr; (c) M2a, magnetite show high concentrations of Ti, V, Cr and HFSE elements for some sample; (d) M1b, magnetite are also low in Ti, V, and Cr content like M1a

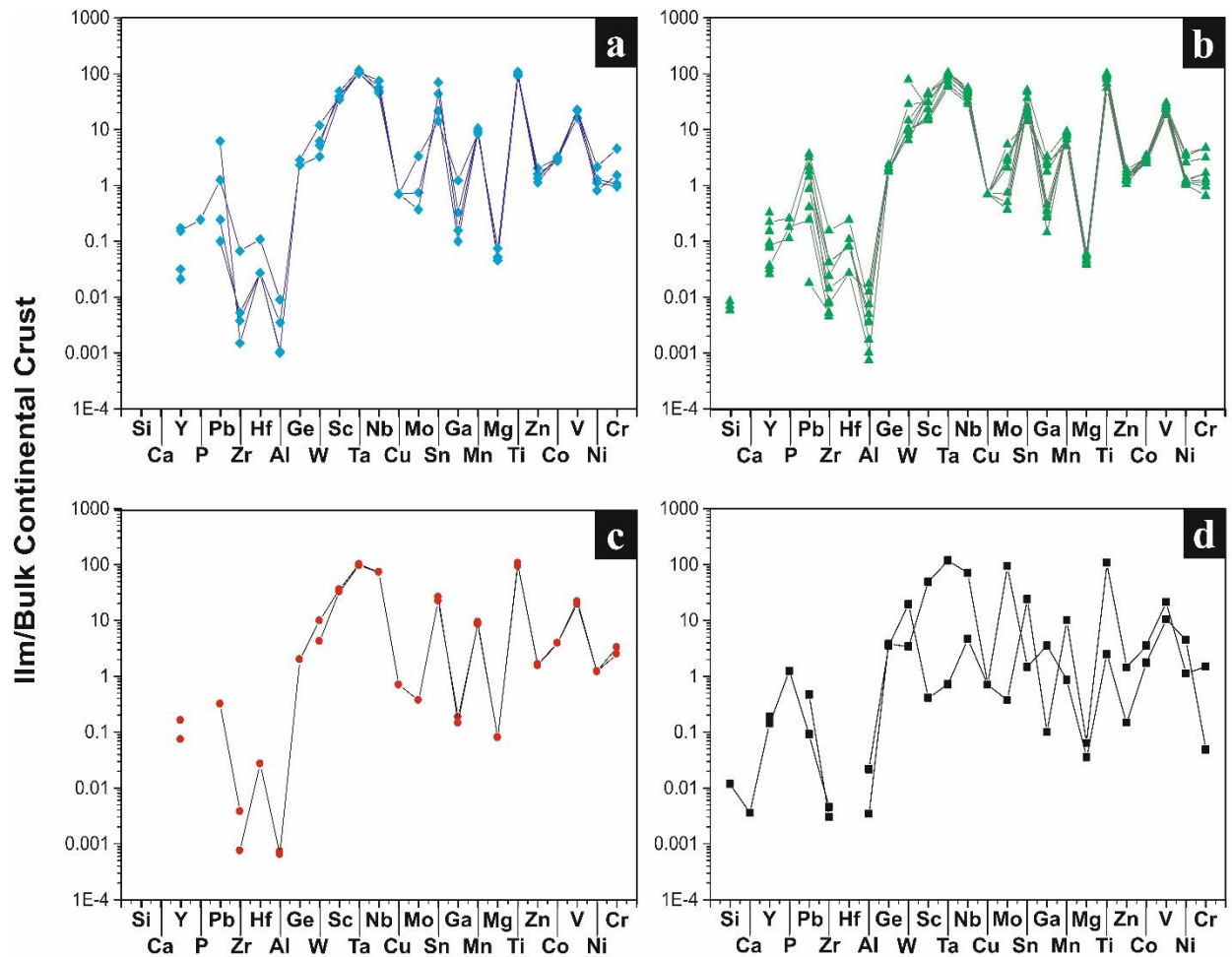


Fig 5.4: (a,b,c,d) Multielement variation diagrams for ilmenite (Ilm), normalized to bulk continental crust (values from Rudnick and Gao 2003). Irrespective of their shape and relationship with the host rock, ilmenite show high concentration of HFSE(Sc, Zr, Hf, Nb, Ta)

Chapter 6: Discussion and Summary:

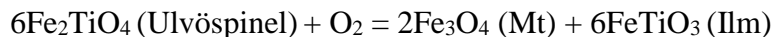
6.1 Introduction:

In the previous chapters, the different textures of magnetite and relationship with associated mineral phases (chapter-3), the geochemical character of magnetite and ilmenite (chapter-4) have been discussed. In this chapter, various magnetite texture along with their geochemical character are implicated and highlighted in terms of their genesis and evolution through time.

In this study, magnetite has two types of occurrences: 1) magnetite + apatite \pm biotite \pm quartz (M1) in the form of vein and 2) magnetite + ilmenite \pm apatite (M2) in the form of massive magnetite body. Apatite-magnetite vein (M1) is further subdivided into apatite-magnetite vein with biotite-quartz (M1a) and apatite-magnetite vein devoid of biotite (M1b). Within the massive magnetite body, most magnetite is associated with ilmenite exsolution lamellae (M2a). In contrast, within the same massive magnetite pocket, there are some magnetite which are devoid of ilmenite exsolution lamella (M2b).

6.2 Ilmenite lamella: primary vs. secondary exsolution

It has been proposed by Buddington and Lindsley (1964) that at high temperature ($\sim 900^\circ\text{C}$) and high $f\text{O}_2$ condition, ilmenite can form directly from Fe_2TiO_4 component of the melt above the solvus of ulvöspinel-magnetite. In such case ilmenite and magnetite co-crystallizes. This process is known as primary oxy-exsolution (Buddington and Lindsley, 1964). In such a case it is expected that the rock will contain independent and isolated grains of ilmenite and magnetite that may often show equilibrium texture between them. In the present case most ilmenites, barring the exceptions of re-equilibrated grains (Chapter 3), occur as exsolved lamella restricted well within magnetite. The lamellae have definite pattern and follow specific crystallographic direction. Therefore, it is proposed that the observed texture did not form by primary oxy-exsolution at high temperature. Alternatively, ilmenite can exsolve from ulvöspinel at temperature below 600°C by the following reaction.



This process is known as secondary oxidation-exsolution. Such a mechanism will result in the formation of ilmenite lamella in a magnetite host as seen in the present case. Therefore, it is proposed that intergrowth texture seen between magnetite-ilmenite is the result of low temperature oxidation. There are sandwich and composite type of ilmenite which are reported to have formed by both primary and secondary exsolution process (Buddington and Lindsley 1964, Haggerty 1991). It may be noted that the composite type ilmenite that are present in the studied sample has crude orientation suggesting their formation from existing oriented lamella. Therefore, the ilmenite-magnetite textural relation as described in this study is best explained by low-temperature secondary exsolution.

6.2 Explanations for compositional variations among different types of magnetite:

The concentration of an element in magnetite depends on several factors such as (a) primary element concentration in melt/fluid from which it crystallizes, (b) a competitive environment, where co-crystallization of other mineral phases competes for geochemically similar elements, (c) partition-coefficient (D) of the element in between magnetite and melt/fluid from which it grows. These factors depend on different physicochemical parameters such as temperature, oxygen fugacity and cooling rate (Mollo et al. 2013, Nadoll et al. 2014, Dare et al. 2014).

The magnetite associated with ilmenite (M2a) has high content of V (5769-8484 ppm), Cr, and Ni concentration. These concentration ranges are consistent with the global range of igneous magnetite (for example <70-6600 ppm V, Nadoll et al. 2014b). In contrast, magmatically originated magnetite from Bushveld complex that formed at greater depth contains very high V (~13,500 ppm) (Cawthorne and Molyneux, 1986). It may be recalled that the composition of M2a magnetite fall in the field of Porphyry Cu deposits. However, the M2 magnetite is not associated with granite and it contains abundant ilmenite exsolution suggesting their mafic parentage. It is to be noted that ilmenite exsolved from the original spinel mineral (titano-magnetite/ulvospinel). Therefore, If the original composition of these magnetite (originally titano-magnetite/ulvospinel) is considered, the Ti-content would have been much higher and the composition would have fallen in the magmatic Fe-Ti-V field or even beyond. This explains why the Ti-content of this magnetite

is lower shifting the composition to Porphyry Cu field. The M2b magnetite have variable Ni/(Cr+Mn) contents and fall in the fields of Porphyry Cu and Kiruna-type deposits. Some grains have even higher Ni/(Cr+Mn) values similar to the M1 magnetite. This suggest that M2b magnetites were later modified, perhaps by the same fluid that formed the M1 magnetite. It is known that Ni in hydrothermal fluid is more soluble than Cr and therefore hydrothermal magnetite or magnetite modified by hydrothermal process may contain higher Ni. That M2b magnetites were hydrothermally altered is evidenced by the presence abundant biotite along the grain boundary of and fracture in this magnetite.

From the trace element data, M2a and M2b magnetite are distinguished by their Ga concentration (Fig 5.1b, e). Recent studies of Prokof'ev et al. 2016 show that gallium concentrations in magmatic melts vary from 0.47 to 495 ppm at average content of 18.0 ppm (+4.2/-3.4) whereas in natural fluid Ga concentration vary in between 0.02-11,260 ppm with an average value of 1.6 ppm (+10.8/-1.4). Nadoll et al. 2014 also demonstrated the higher concentration of Ga in case of igneous Henderson Climax-type Mo deposit whereas low temperature BIF and iron ore deposits have low concentration of Ga. According to these two studies, M2a crystallized at a higher temperature relative to M2b. So, M2b can be later crystalizing phase and thus contain low Cr, Ti and Ni (Fig 4.1a, c, Fig 5.1b, c, d, e).

The M1a magnetite crystallized from a hydrothermal fluid which is evidenced by the mode of occurrence (in the form of vein) and Ti content and Ni/Cr ratios (Fig 5.2a; Chapter 5; Dare et al. 2014). Nadoll et al. (2014) considered that foreign cations in hydrothermal magnetite are continuously expelled by re-equilibration, leading to higher mass of Fe associated with low Ti, V, Cr concentration, which is characteristic of M1 magnetite in the present study (Fig 4.1 c, d). Ga concentration also distinguishes M1a magnetite from M1b magnetite, both of which are hosted in apatite-magnetite veins. M1b magnetite (without abundant biotite) has a higher concentration of Ga relative to M1a suggesting that M1b forms at a higher temperature relative to M1a.

Partitioning of HFSE elements between exsolved ilmenite and host magnetite

Multielement variation diagram of magnetite and ilmenite are normalized to bulk continental crust (data from Rudnick and Gao, 2003) in increasing order of compatibility of elements in magnetite structure (Fig 5.3, 5.4) (Dare et al. 2014). It is seen that the host magnetite is characterized by low concentration of HFSE (Ti, Zr, Hf, Sc, Nb, and Ta). The exsolved ilmenite phase contains high proportion of HFSE. By comparing these two mineral phases, it is evident that during sub-solidus exsolution element redistribution took place between the exsolved and host phases. Ionic potential of Nb^{4+} , Ta^{4+} , Zr^{4+} , Hf^{4+} , Sc^{4+} is similar to that of Ti^{4+} , so HFSE elements readily substitute Ti^{4+} and Mn^{2+} substitute in place of Fe^{2+} during sub-solidus oxidation. Along with that, this substitution schemes help to understand the primary spinel_{ss} which was initially enriched in Ti, V, Cr, Ni, Co and HFSE elements. Concentrations of HFSE indicates the magma's evolve nature as the HFSE behave as incompatible during melt-crystal partitioning.

References:

- Buddington, A. F., & Lindsley, D. H. (1964). Iron-titanium oxide minerals and synthetic equivalents. *Journal of petrology*, 5(2), 310-357.
- Cawthorn, R. G., & Molyneux, T. G. (1986). Vanadiferous magnetite deposits of the Bushveld Complex. *Mineral deposits of Southern Africa. Geol Soc S Afr Johannesburg*, 2, 1251-1266.
- Chen, W. T., Zhou, M. F., Li, X., Gao, J. F., & Hou, K. (2015). In-situ LA-ICP-MS trace elemental analyses of magnetite: Cu-(Au, Fe) deposits in the Khetri copper belt in Rajasthan Province, NW India. *Ore Geology Reviews*, 65, 929-939.
- Dare, S. A., Barnes, S. J., Beaudoin, G., Méric, J., Boutroy, E., & Potvin-Doucet, C. (2014). Trace elements in magnetite as petrogenetic indicators. *Mineralium Deposita*, 49(7), 785-796.
- Dunn, J. A., & Dey, A. K. (1942). The geology and petrology of eastern Singhbhum and surrounding areas (Vol. 69). Government of India Press.
- Dupuis, C., & Beaudoin, G. (2011). Discriminant diagrams for iron oxide trace element fingerprinting of mineral deposit types. *Mineralium Deposita*, 46(4), 319-335.
- Fleet, M. E. (1981). The structure of magnetite. *Acta Crystallographica Section B: Structural Crystallography and Crystal Chemistry*, 37(4), 917-920.
- Ghiorso, M. S., & Sack, O. (1991). Fe-Ti oxide geothermometry: thermodynamic formulation and the estimation of intensive variables in silicic magmas. *Contributions to Mineralogy and Petrology*, 108(4), 485-510.
- Haggerty, S. E. (1991). Oxide Textures-A mini-atlas. *Oxide Minerals, Petrologic and magnetic significance*, 129-137.
- Knipping, J. L., Bilenker, L. D., Simon, A. C., Reich, M., Barra, F., Deditius, A. P., ... & Munizaga, R. (2015). Trace elements in magnetite from massive iron oxide-apatite deposits indicate a combined formation by igneous and magmatic-hydrothermal processes. *Geochimica et Cosmochimica Acta*, 171, 15-38.
- Lindsley, D. H. (1976). The crystal chemistry and structure of oxide minerals as exemplified by the Fe-Ti oxides. *Oxide minerals*, L1-L60.
- McClenaghan, M. B. (2005). Indicator mineral methods in mineral exploration. *Geochemistry: Exploration, Environment, Analysis*, 5(3), 233-245.
- Misra, S. (2006). Precambrian chronostratigraphic growth of Singhbhum-Orissa craton, Eastern Indian shield: an alternative model. *JOURNAL-GEOLOGICAL SOCIETY OF INDIA*, 67(3), 356.

- Mollo, S., Putirka, K., Iezzi, G., & Scarlato, P. (2013). The control of cooling rate on titanomagnetite composition: implications for a geospeedometry model applicable to alkaline rocks from Mt. Etna volcano. *Contributions to Mineralogy and Petrology*, 165(3), 457-475.
- Nadoll, P., Angerer, T., Mauk, J. L., French, D., & Walshe, J. (2014). The chemistry of hydrothermal magnetite: a review. *Ore geology reviews*, 61, 1-32.
- Nadoll, P., Mauk, J. L., Leveille, R. A., & Koenig, A. E. (2014b). Geochemistry of magnetite from porphyry Cu and skarn deposits in the southwestern United States. *Mineralium Deposita*, 50(4), 493-515.
- Naha, K. (1965). A critique of “orogenic trends” in Archaean correlation in India. *Tectonophysics*, 1(5), 431-438.
- Pal, D. C., Barton, M. D., & Sarangi, A. K. (2009). Deciphering a multistage history affecting U–Cu (–Fe) mineralization in the Singhbhum Shear Zone, eastern India, using pyrite textures and compositions in the Turamdih U–Cu (–Fe) deposit. *Mineralium Deposita*, 44(1), 61-80.
- Pal, D. C., Chaudhuri, T., McFarlane, C., Mukherjee, A., & Sarangi, A. K. (2011). Mineral chemistry and in situ dating of allanite, and geochemistry of its host rocks in the Bagjata Uranium Mine, Singhbhum Shear Zone, India—implications for the chemical evolution of REE mineralization and mobilization. *Economic Geology*, 106(7), 1155-1171.
- Pal, D. C., Trumbull, R. B., & Wiedenbeck, M. (2010). Chemical and boron isotope compositions of tourmaline from the Jaduguda U (–Cu–Fe) deposit, Singhbhum shear zone, India: implications for the sources and evolution of mineralizing fluids. *Chemical Geology*, 277(3-4), 245-260.
- Prokof'ev, V. Y., Naumov, V. B., & Dorofeeva, V. A. (2016). Gallium concentration in natural melts and fluids. *Geochemistry International*, 54(8), 691-705.
- Ramakrishnan, M., Vaidyanadhan, R. (2010). *Geology of India* (vol. 1), Geological Society of India.
- Ramdohr, P. (1980) *The ore minerals and their intergrowth*, 2nd edition. International Series in Earth Science, Academic Press, New York, United States.
- Razjigaeva, N. G., & Naumova, V. V. (1992). Trace element composition of detrital magnetite from coastal sediments of northwestern Japan Sea for provenance study. *Journal of Sedimentary Research*, 62(5), 802-809.
- Rudnick, R. L., & Gao, S. (2003). Composition of the continental crust. *Treatise on geochemistry*, 3, 659.
- Saha, A. K. (1994). *Crustal evolution of Singhbhum-North Orissa, eastern India*. GSI Publications, 1(1).

- Saha, A. K., & Ray, S. L. (1984). The structural and geochemical evolution of the Singhbhum granite batholithic complex, India. *Tectonophysics*, 105(1-4), 163-176.
- Sarkar, S. C. (1984). *Geology and ore mineralization along the Singhbhum copper uranium belt, Eastern India*. Jadavpur University, Calcutta.
- Sarkar, S. C., & Gupta, A. (2012). *Crustal evolution and metallogeny in India*. Cambridge University Press.
- Sarkar, S. C., Deb, M. (1974). Metamorphism of Sulfides of the Singhbhum Copper Belt, India; The Evidence from the Ore Fabric. *Economic Geology* ; 69 (8): 1282–1293
- She, Y. W., Song, X. Y., Yu, S. Y., & He, H. L. (2015). Variations of trace element concentration of magnetite and ilmenite from the Taihe layered intrusion, Emeishan large igneous province, SW China: Implications for magmatic fractionation and origin of Fe–Ti–V oxide ore deposits. *Journal of Asian Earth Sciences*, 113, 1117-1131.
- Talapatra, A.K. (1948). Sulfide mineralization associated with migmatization in the southeastern part of the Singhbhum shear zone, Bihar, India. *Econ Geol* 63, 156-165.
- Tan, W., Liu, P., He, H., Wang, C. Y., & Liang, X. (2016). Mineralogy and origin of exsolution in Ti-rich magnetite from different magmatic Fe-Ti oxide-bearing intrusions. *The Canadian Mineralogist*, 54(3), 539-553.
- Toplis, M. J., & Corgne, A. (2002). An experimental study of element partitioning between magnetite, clinopyroxene and iron-bearing silicate liquids with particular emphasis on vanadium. *Contributions to Mineralogy and Petrology*, 144(1), 22-37.
- Watenphul A., Schmidt C. and Scholten L. (2012) First insights into Cr^{3+} solubility in aqueous fluids at elevated P and T by I-XRF. 1st European Mineralogical Conference – EMC. Frankfurt, Germany #544 (abstr.).
- Watenphul A., Scholten L, Kavner A., Alraun P., Falkenberg G., Newville M., Lanzirotti A. and Schmidt C. (2013) Cu and Ni solubility in high-temperature aqueous fluids. American geophysical Union – AGU, Fall meeting. San Francisco, CA, USA #MR33A-2311 (abstr.).University Press.
- Waychunas, G. A. (1991). Crystal chemistry of oxides and oxyhydroxides. *Oxide minerals: Petrology and magmatic significance*, 11-68.
- Wechsler, B. A., Lindsley, D. H., & Prewitt, C. T. (1984). Crystal structure and cation distribution in titanomagnetites ($\text{Fe}_{3-x}\text{Ti}_x\text{O}_4$). *American Mineralogist*, 69(7-8), 754-770.